Research Square

Preprints are preliminary reports that have not undergone peer review.
They should not be considered conclusive, used to inform clinical practice,
or referenced by the media as validated information.

Gut microbial interaction networks control autoimmunity to neuroretina

Amy Zhang*
Laboratory of Immunology, National Eye Institute, National Institutes of Health, Bethesda, MD, USA
Reiko Horai*
hreiko@NIH.gov
Laboratory of Immunology, National Eye Institute, National Institutes of Health, Bethesda, MD, USA
Yingyos Jittayasothorn
Laboratory of Immunology, National Eye Institute, National Institutes of Health, Bethesda, MD, USA
Jonathan H. Badger
Genetics and Microbiome Core, Laboratory of Integrative Cancer Immunology, Center for Cancer Research, National Cancer Institute, National Institutes of Health, Bethesda, MD, USA
https://orcid.org/0000-0002-5662-423X
Zhichao Wu
Laboratory of Pathology, Center for Cancer Research, National Cancer Institute, National Institutes of Health, Bethesda, MD, USA
Guangpu Shi
Laboratory of Immunology, National Eye Institute, National Institutes of Health, Bethesda, MD, USA
Akriti Gupta
Laboratory of Immunology, National Eye Institute, National Institutes of Health, Bethesda, MD, USA
Samyuktha Arunkumar
Laboratory of Immunology, National Eye Institute, National Institutes of Health, Bethesda, MD, USA
Caitlin E. Murphy
Laboratory of Immunology, National Eye Institute, National Institutes of Health, Bethesda, MD, USA
Vijayaraj Nagarajan
Laboratory of Immunology, National Eye Institute, National Institutes of Health, Bethesda, MD, USA
John A. McCulloch
Genetics and Microbiome Core, Laboratory of Integrative Cancer Immunology, Center for Cancer Research, National Cancer Institute, National Institutes of Health, Bethesda, MD, USA
Shilpa Kodati
Laboratory of Immunology, National Eye Institute, National Institutes of Health, Bethesda, MD, USA
Hatice Nida Sen
Laboratory of Immunology, National Eye Institute, National Institutes of Health, Bethesda, MD, USA
Jung-Wha Lee

Laboratory of Immunology, National Eye Institute, National Institutes of Health, Bethesda, MD, USA

Jonathan P. Jacobs

Goodman-Luskin Microbiome Center, David Geffen School of Medicine at UCLA, Los Angeles, CA, USA https://orcid.org/0000-0003-4698-0254

Xiaoyan Xu

Laboratory of Immunology, National Eye Institute, National Institutes of Health, Bethesda, MD, USA

Mary J. Mattapallil

Laboratory of Immunology, National Eye Institute, National Institutes of Health, Bethesda, MD, USA https://orcid.org/0000-0003-0615-7343

Zixuan Peng

Laboratory of Immunology, National Eye Institute, National Institutes of Health, Bethesda, MD, USA

Biying Xu

Laboratory of Immunology, National Eye Institute, National Institutes of Health, Bethesda, MD, USA

Robert J. Palmer

Structural Biochemistry Unit, National Institute of Dental and Craniofacial Research, National Institutes of Health, Bethesda, MD, USA

Nadim Majdalani

Laboratory of Molecular Biology, Center for Cancer Research, National Cancer Institute, National Institutes of Health, Bethesda, MD, USA https://orcid.org/0000-0002-9314-5203

Kenya Honda

Keio University School of Medicine, Tokyo, Japan https://orcid.org/0000-0001-8937-9835

Colm O'hUigin

Genetics and Microbiome Core, Laboratory of Integrative Cancer Immunology, Center for Cancer Research, National Cancer Institute, National Institutes of Health, Bethesda, MD, USA

Rachel R. Caspi

caspir@nei.nih.gov

Laboratory of Immunology, National Eye Institute, National Institutes of Health, Bethesda, MD, USA https://orcid.org/0000-0002-7140-7671

Biological Sciences - Article

Keywords: Gut microbiome, Autoimmune uveitis, Akkermansia, Short-chain fatty acids, Th1 effector response, human flora

Posted Date: May 4th, 2026

DOI: https://doi.org/10.21203/rs.3.rs-9528424/v1

License: This work is licensed under a Creative Commons Attribution 4.0 International License.
Read Full License

Additional Declarations: There is **NO** Competing Interest.

Gut microbial interaction networks control autoimmunity to neuroretina

Amy Zhang[1#], Reiko Horai[1#*], Yingyos Jittayasothorn[1], Jonathan H. Badger[2], Zhichao Wu[3], Guangpu Shi[1], Akriti Gupta[1], Samyuktha Arunkumar[1], Caitlin E. Murphy[1], Vijayaraj Nagarajan[1], John A. McCulloch[2], Shilpa Kodati[1], H Nida Sen[1], Jung Wha Lee[1], Jonathan P. Jacobs[4], Xiaoyan Xu[1], Mary J. Mattapallil[1], Zixuan Peng[1], Biying Xu[1], Robert J. Palmer[5], Nadim Majdalani[6], Kenya Honda[7], Colm O'hUigin[2], Rachel R. Caspi[1*]

[1]Laboratory of Immunology, National Eye Institute, National Institutes of Health, Bethesda, MD, USA

[2]Genetics and Microbiome Core, Laboratory of Integrative Cancer Immunology, Center for Cancer Research, National Cancer Institute, National Institutes of Health, Bethesda, MD, USA

[3]Laboratory of Pathology, Center for Cancer Research, National Cancer Institute, National Institutes of Health, Bethesda, MD, USA

[4]Goodman-Luskin Microbiome Center, David Geffen School of Medicine at UCLA, Los Angeles, CA, USA

[5]Structural Biochemistry Unit, National Institute of Dental and Craniofacial Research, National Institutes of Health, Bethesda, MD, USA

[6]Laboratory of Molecular Biology, Center for Cancer Research, National Cancer Institute, National Institutes of Health, Bethesda, MD, USA

[7]Keio University School of Medicine, Tokyo, Japan

[#]Equal contribution

*Correspondence to:

Rachel R. Caspi (caspir@nei.nih.gov)

Laboratory of Immunology, National Eye Institute, National Institutes of Health
10 Center Drive, 10/10N248, Bethesda, MD 20892-1857, USA

Reiko Horai (hreiko@nih.gov)

Laboratory of Immunology, National Eye Institute, National Institutes of Health
10 Center Drive, 10/10S243, Bethesda, MD 20892-1857, USA

Running title: Gut microbial interactions drive autoimmune uveitis

Funding: NIH/NEI Intramural funding, Project Number EY000184

Commercial Disclosures: None

KEYWORDS

Gut microbiome, Autoimmune uveitis, Akkermansia, Short-chain fatty acids, Th1 effector response, human flora

ABSTRACT

The gut microbiome influences the development of immune-mediated inflammatory diseases, including autoimmune uveitis, a sight-threatening ocular inflammation driven by retina-specific T cells[1]. Using a model of spontaneous autoimmune uveitis (sEAU) we showed that gut commensals provide immune stimuli that trigger disease[2]. Here we report that uveitis-promoting microbes are present in human gut flora and that colonization of germ-free (GF) mice with commensals from healthy human donors was sufficient to provoke disease. Severity of sEAU correlated with expansion of Akkermansia and contraction of short-chain fatty acid (SCFA)–producing Firmicutes, followed by decreased SCFA levels and a dominant gut Th1 effector response. Mechanistic gain-of-function experiments, enriching GF sEAU mice with Akkermansia, reproduced these microbiome, metabolite and immune phenotype shifts, and exacerbated disease, suggesting that Akkermansia promotes autoimmunity by outcompeting SCFA-producers and enhancing Th1-type responses. An inverse correlation between Akkermansia (Verrucomicrobia) and Firmicutes was also present in patients with uveitis, multiple sclerosis and Crohn's disease. These findings reveal a stereotypic gut microbial interaction network that regulates systemic immune balance, and may represent an ecologically conserved mechanism through which the gut microbiome modulates autoimmune and inflammatory diseases.

INTRODUCTION

Immune-privileged tissues are increasingly recognized as sites where host–microbiota interactions influence immunological balance in autoimmune and inflammatory diseases[3,4]. Multiple mechanisms have been proposed that explain the central role of microbiota in driving inflammation in the central nervous system (CNS), including innate and adaptive effects such as molecular mimicry[2,5], bystander activation[6], epitope spreading[7,8] and dual T cell receptors (TCRs)[9]. The eye, especially the neuroretina, is part of the CNS and represents a quintessential immune-privileged tissue, making it a valuable model to study immune privilege and autoimmunity in the CNS.

Autoimmune uveitis is a T cell-driven intraocular inflammation of unknown etiology that targets the neuroretina and can lead to blindness[1]. It is represented by the models of experimental autoimmune uveitis (EAU) in animals. EAU is induced in wild type mice by immunization with the retinal antigen IRBP[1], or can develop spontaneously (sEAU) in mice expressing a transgenic IRBP-specific TCR cloned from the immunization induced model (line R161H)[10]. Our previous studies highlighted the critical role of gut microbiome in triggering sEAU by providing antigenic stimuli that activate retina-specific T cells[2]. Subsequent research reported inhibitory effects of microbiome depletion also in induced EAU[11], where the antigen is provided, emphasizing the antigen-independent (innate?) effects of gut microbes on EAU. Interestingly, gut microbiome studies in uveitis patients have revealed differences in gut flora between patients and healthy controls[12-16], but mechanistic information could not be resolved.

Because inductive events and causal relationships cannot be studied in patients, we employed the model of sEAU in R161H TCR transgenic mice[10], which may provide a more physiological system to study triggers delivered by the microbiota. To gain mechanistic insights into how human gut microbiota might affect the development of autoimmune uveitis, we created gnotobiotic breeding colonies of R161H mice harboring healthy human gut flora by reconstituting GF parental mice with fecal material from three healthy human donors. The rationale for focusing on healthy donors is that *(i)* every uveitis patient was once a healthy person, so by definition, uveitis-relevant microbes should be present in the healthy person's gut flora, and *(ii)* the composition of patient

flora could have been altered by their disease or by their treatment, confounding data interpretation.

Using a multiomic strategy that integrates microbial, metabolomic and immune profiling of human flora (HuFl)-reconstituted R161H mice, combined with analyses of human autoimmune disease datasets, we identified a microbial interaction network comprising an "Akkermansia/Verrucomicrobia—Firmicutes axis" that appears to regulate autoimmunity. Our data points to an underexplored but fundamental mechanism, where interactive relationships in the microbial community play a central role in regulation of autoimmune disease pathogenesis by microbiota[17].

RESULTS

1. Human gut commensals support development of spontaneous experimental autoimmune uveitis (sEAU)

R161H mice harboring mouse microbiota (specific-pathogen-free, SPF) typically develop moderate to severe uveitis with high penetrance (100% incidence by two months of age)[10]. To first assess whether human gut microbiota affect uveitis development, we developed "humanized gnotobiotic" R161H mouse lines as our pre-clinical model, by reconstituting breeding pairs of GF R161H mice with gut microbiota from three healthy human subjects—U, V, and W. Each line was maintained in separate isolators through successive generations, so that the offspring acquired the human flora naturally from their respective parents (Fig. 1a).

Microbiome sequencing results showed successful engraftment of human flora in gnotobiotic R161H mice. The succession of gut microbiota through generations of breeding in gnotobiotic isolators did not appear to diminish the differences between individual cohorts, and each U, V, or W mouse recipient cohort preserved the microbial signatures of its original donor (Fig. 1b).

Human commensal microbes supported uveitis development in R161H mice. Although HuFl mice display a broad spectrum of disease scores, the scores were on average lower than those of SPF mice that harbor normal mouse flora (Fig. 1c & Extended Data Fig. 1a). We did not observe obvious sex differences with respect to disease severity in HuFl mice (Extended Data Fig. 1b). Immune phenotype of colonic $CD4^+$ T cells, based on a range of cell surface and intracellular markers, clearly distinguished HuFl mice from GF and SPF mice (Fig 1d & Extended Data Fig. 1c-e). The HuFl mice showed a spectrum of disease scores and memory marker expression between GF (low) and SPF (high) mice (Fig. 1e), had fewer IFN-γ-producing Th1 and IL-17A-producing Th17 effector cells and more regulatory T cells (Tregs) expressing Foxp3 and IL-10 than did SPF mice (Fig. 1f-g). This immune phenotype was consistent with other activation markers and Th1/Th17 signature molecules (Extended Data Fig. 1e). This phenotype may explain the lower disease scores that they developed.

2. HuFl sEAU tracks with a dominant Th1 phenotype and abundance of Verrucomicrobia/Akkermansia

Since both Th1 and Th17 effector phenotypes can drive autoimmune uveitis[18-20], we set out to define the immune signatures that associate with disease in the HuFl model. We categorized histological scores into high (score ≥ 1.5), mid (0.75 < score < 1.5), and low (score ≤ 0.75) to facilitate statistical analysis. Interestingly, IFN-γ-producing CD4 T cells, rather than IL-17A producers, in the gut (and other tissues) associated strongly with severe disease phenotype (Fig. 2a-d). This suggests that uveitis development in HuFl mice is more dependent on Th1 than Th17.

Microbiome analysis of parental and offspring HuFl mice showed that colonized mice adopted only a subset of the original donor taxa (Extended Data Fig. 2a-b). This could be a result from loss during human stool sample preservation and transfer processes, and/or from inefficient engraftment of some non-native microbes to the gut environment of a different host species. However, in terms of the overall microbial composition, each mouse cohort remained closer to their original donor, preserving a distinct microbial footprint (Fig. 1b & Extended Data Fig. 2c-d). Differences between female *vs.* male HuFl mice in terms of microbial abundance and composition were minimal, if any, compared to

the differences based on human donors (Extended Data Fig. 2e-f). This is compatible with the apparent lack of sex differences in disease severity of HuFl mice (Extended Data Fig. 1b).

We then explored how gut microbiome associates with severity of uveitis. Correlational heat map of major bacterial taxa at the family level revealed strong links between several taxa and histology scores (Fig. 2e). Among them, Akkermansia (the only representative of Verrucomicrobia in HuFl mice) correlated with high disease scores (Pearson r = 0.5, FDR <0.05), whereas certain members of the Firmicutes phylum were correlated with low disease scores (Pearson r = -0.3, FDR <0.05). Differential abundance analysis between high and low histology categories consistently showed that Akkermansia was enriched in mice with high disease, whereas Firmicutes (especially Clostridia) were enriched in mice with low disease (Fig. 2f-g & Extended Data Fig. 2g).

3. SCFA signatures are enriched in low disease HuFl mice or healthy subjects

SCFAs are metabolites of commensal gut microbes resulting from fermentation of dietary fiber, and have anti-inflammatory properties in a range of pathological conditions[21]. Some SCFAs, e.g. butyrate and propionate, may have therapeutic potential in induced EAU[22,23]. In the current study, a key observation from differential abundance analyses of mice with low and high disease scores was that SCFA-producing Firmicutes were associated with lower sEAU scores (Fig. 2e). Therefore, it appeared plausible that SCFAs may also have the potential to modulate sEAU.

To address this, we mined functional gene signatures from shotgun metagenomic sequences of HuFl mice. Genes known to be involved in SCFAs synthesis and metabolism were mapped to the simplified pathways shown in Fig. 3a. Consistent with the observed differences in microbial abundance (Fig. 2e), the genes involved in main SCFA pathways were enriched in mice with low disease scores and reduced in mice with high disease scores (Fig. 3b). In agreement with the pathway analysis, metabolomic quantification of SCFAs in the gut and serum of the mice confirmed that higher disease scores were associated with lower SCFA concentrations both locally and systemically (Fig. 3c).

We next examined whether this signature was present in a cohort of uveitis patients seen at the National Eye Institute (NEI) clinic, compared to healthy controls. Because uveitis is a heterogenous disease, we focused on a subset of patients whose disease was restricted to the eye (idiopathic uveitis, Vogt-Koyanagi-Harada disease/sympathetic ophthalmia and birdshot chorioretinopathy), as modeled by EAU, rather than being part of a systemic syndrome. Similarly to the HuFl R161H mice, enzymes involved in acetate, butyrate and propionate pathways (Fig. 3d) and their corresponding SCFAs (Fig. 3e), were reduced in uveitis patients compared to healthy controls. This supports a role for SCFAs in regulation of human uveitis.

4. Akkermansia negatively correlates with Firmicutes in both sEAU and clinical uveitis

Among all taxa in HuFl mice, Akkermansia abundance was shown to be a prominent correlate of severe uveitis and IFN-γ-producing CD4+ T cells in the gut (Fig. 2e-f, Extended Data Fig. 3a–b), whereas SCFA-producing Firmicutes were reduced in the same animals (Fig. 2e, g). We therefore analyzed their relative abundance and potential interdependence to determine whether competitive interactions between these taxa might contribute to autoimmune uveitis.

We first quantified abundance of Akkermansia and Firmicutes, and found them to be inversely correlated (Fig. 4a). An in-depth computational analysis of the bacterial association network confirmed the negative correlation between Akkermansia and multiple families of SCFA-producing Firmicutes (Fig. 4b, Extended Data Fig. 3c). Levels of major SCFAs in feces also exhibited an inverse correlation with Akkermansia abundance (Fig. 4c). Taken together, this supports an interpretation of a negative interaction between Akkermansia and a range of SCFA-producing microbes.

Similarly, gut microbiome interaction networks of uveitis patients displayed a negative relationship between Verrucomicrobia (primarily Akkermansia) and SCFA-producing Firmicutes (Clostridia, class level), but this relationship was not evident in healthy subjects (Fig. 4d). This supports the relevance of the sEAU model to clinical disease.

5. Akkermansia promotes uveitis by outcompeting SCFA producers and decreasing circulating SCFA levels

To validate the proposed microbiome interaction network *in vivo*, we used a gain-of-function approach, where GF R161H mice received Akkermansia alone or Akkermansia mixed with HuFl mouse donor fecal flora. In the first paradigm, we associated GF mice *de novo* with cultured *Akkermansia muciniphila* (the type species of Akkermansia) or with sterile PBS as control, and maintained them in static microisolators using sterile handling techniques, to minimize additional microbial exposure (Extended Data Fig. 4a). This approach resulted in a minimal gut microbial population of very low diversity (≤10 total detectable taxa/mouse), dominated by Verrucomicrobia (Akkermansia) and Firmicutes (Extended Data Fig. 4b-d).

First paradigm: A single oral gavage led to successful and sustained engraftment of Akkermansia, and resulted in higher uveitis scores (Extended Data Fig. 4e-f). Akkermansia was nearly undetectable in the PBS control group, whose gut microbiota became dominated by Firmicutes (Extended Data Fig. 4g). As such, the relative abundances of Akkermansia and Firmicutes showed a near-perfect inverse relationship (r-squared > 0.99, $p < 0.0001$) (Extended Data Fig. 4h). Other bacterial phyla that are prominent in normal mouse or human gut flora were low or on the borderline of detectability (Extended Data Fig. 4i). Thus, this model reflects a minimal-diversity gut ecosystem dominated by the two taxa that we hypothesize to display competitive dynamics that control expression of disease.

Second paradigm: To examine this hypothesis under more physiological conditions, where Akkermansia is not given a major “head start”, we associated GF R161H mice with flora from HuFl mice (selected for low disease and low abundance of Akkermansia) “spiked”, or not, with cultured *A. muciniphila* (Fig. 5a). Fecal microbiome profiling confirmed successful microbial engraftment and stability of Akkermansia-high or Akk-low status (Fig. 5d & Extended Data Fig. 5a). Akkermansia “spiked” flora induced more severe uveitis than base HuFl alone (Fig. 5b-c) and the relative abundances of Akkermansia and Firmicutes were consistently inversely correlated (Fig. 5e). Notably, among the major bacterial phyla,

Firmicutes was the only phylum whose abundance was decreased in Akk-enriched mice (Fig. 5d & Extended Data Fig. 5b), particularly those taxa considered “professional” SCFA producers[24] (Extended Data Fig. 5c). To confirm that the effects described above were indeed Akkermansia-specific, we associated GF R161H mice with the same HuFl “spiked” with *E. coli*. The disease-promoting phenotype and the reduction in Firmicutes abundance were not recapitulated, supporting the notion that the observed effects were specific to Akkermansia (Extended Data Fig. 5d-f). Together, these results reinforce a dynamic balance between Akkermansia and Firmicutes that modulates autoimmune uveitis in a physiologically relevant setting.

To mechanistically link Akkermansia–Firmicutes dynamics with circulating SCFA levels available to regulate uveitis-relevant immune responses, we measured serum SCFAs and host immune parameters. All three major SCFAs – acetic, butyric and propionic acids – were reduced in Akk-high mice compared with Akk-low mice (Fig. 5f), consistent with the negative relationship between Akkermansia and Firmicutes. This reduction was not observed in the *E.coli* control group (Extended Data Fig. 5g). Given the known immunomodulatory role of SCFAs[21] , we examined whether this metabolomic shift was associated with an altered systemic effector response. In both the Akk-associated minimal flora model and the Akk-enriched HuFl model, reduced serum SCFAs were tightly coupled with elevated serum and/or gut IFN-γ responses (Fig. 5g–j). These results implicate that SCFAs may regulate disease by dampening the Th1 effector response.

The final mechanistic question was whether Akkermansia can provide surrogate antigenic stimuli to trigger activation of the R161H TCR-expressing cells in the gut[2]. To address this, we used an *in vitro* activation assay, where naïve R161H CD4 T cells and antigen-presenting cells were cultured with Akk-rich HuFl gut content extracts, or with heat-killed Akkermansia. Unlike SPF gut flora extracts or the cognate peptide antigen[2,10], neither Akkermansia preparation activated the retina-specific T cells, as measured by expression of CD69 and Nur77 (Extended Data Fig. 6a-b), indicating that Akkermansia was not acting as an antigen mimic.

Single cell RNA-seq analysis of colonic CD4 T cells, of which an average of 15% expressed the R161H TCR, revealed that both R161H TCR-expressing and non-R161H (endogenous) T cells had a Th1, rather than a Th17, signature, that positively correlated with abundance of Akkermansia (Extended Data Fig. 6c). Akk-high colonic CD4 T cells showed an increased proportion of Th1 cells with enriched interferon- and inflammation-associated transcriptional programs (Stat1, Irf1, Cebpb, Jund), indicating an augmented Th1 transcriptional profile (Extended Data Fig. 6d-e) and a broadly increased myeloid-to-T cell signaling (Extended Data Fig. 6f), in which MHC class-II-associated APC–CD4 interactions favor Type 1 over Type 17 polarization (Extended Data Fig. 6g).

VDJ analysis did not reveal evidence for a 2nd TCR among R161H TCR+ cells, and *in silico* analysis did not reveal shared sequence(s) between Akkermansia and IRBP$_{161\text{-}180}$, which is the cognate R161H TCR epitope, supporting a mechanism independent of cognate antigen recognition. Together, these findings support a model in which Akkermansia regulates disease and shapes the T-cell effector response at 2 levels: directly, through innate, adjuvant-like mechanisms modulating APC-T cell interactions, as well as indirectly, by modulating SCFA-producing Firmicutes. This working model is depicted in Figure 6a.

6. The inverse relationship between Verrucomicrobia and Firmicutes extends to clinical uveitis, multiple sclerosis and Crohn's disease

Because effector Th1 skewing in the Akk-rich gut environment was independent of antigenic specificity, we hypothesized that it could be associated with human inflammatory conditions, such as uveitis, multiple sclerosis (MS) and inflammatory bowel disease (IBD). To establish a common metric for comparing healthy to diseased state, we used the phylum-level ratio of Verrucomicrobia / Firmicutes (V/F ratio) which consistently tracked with disease severity in HuFl mice (Fig. 6b-c). Application of this metric to the entire cohort of our clinical uveitis samples (so as to minimize any selection bias), revealed higher V/F ratios in uveitis patients compared to healthy subjects (Fig. 6d). We next examined publicly available MS[25] and IBD[26] datasets, the latter comprising patients with Crohn's disease and ulcerative colitis (UC). Compared to healthy controls, the V/F

ratio in MS, and in Crohn's disease patients—a condition predominantly driven by Th1-mediated inflammation—but not in UC patients[27,28], was markedly elevated (Fig. 6e-f). Taken together, the gut microbial interaction networks indicated a negative correlation of Verrucomicrobia (Akkermansia) with Firmicutes not only in R161H mice, but also in uveitis, MS and Crohn's disease patients, supporting the generality of this relationship.

DISCUSSION

In this study, we report a gut microbial interaction network that regulates autoimmune and inflammatory processes along the "gut–eye axis". By integrating data-driven analyses and *in vivo* microbial perturbation, we provide compelling evidence for a negative relationship between Akkermansia and Firmicutes and link it to disease severity. Specifically, Akkermansia appears to promote sEAU in HuFI R161H mice by outcompeting SCFA-producing Firmicutes in the gut, resulting in diminished SCFA levels and enhanced Th1 responses both locally and systemically (Fig. 6a). Our findings provide a mechanistic basis for how the gut microbiome impacts ocular autoimmunity, dissect the complex interacting stimuli that underpin this process, and highlight its broadly generalizable nature.

Our network-based perspective contrasts with previous studies, which have mostly focused on how individual gut microbial taxa influence disease and host immunity[4]. *A. muciniphila* has been implicated across a spectrum of inflammatory and autoimmune diseases[29]. However, different reports have described conflicting functional effects. As an example, Akkermansia has been reported to promote Th1 polarization of human PBMCs[30], and its relative abundance correlated with disease activity in MS patients[25,30-32]. In contrast, in vivo Th1-polarizing activity has not been observed in Akk-monocolonized mice[30] and T cell responses to Akkermansia in SPF mice have not correlated with a consistent T cell effector phenotype[33]. These observations, together with our finding that Akkermansia affects sEAU through interactions that modulate the broader microbial network, support the notion that the immunological impact of

Akkermansia—and of any single microbes in general—depends heavily on microbial community context and host factors.

The R161H sEAU model provides a platform to dissect these contextual effects. When the model was first established, we identified signaling by a (microbiota-dependent) mimic antigen in the SPF flora of R161H mice as an important, but possibly not the only, disease trigger[2]. In the case of Akkermansia as a disease-promoting influence that does not appear to act as a surrogate antigen, it is likely that other HuFl member(s) may provide this function. The preferential enhancement of MHC-II–associated APC–CD4 interactions in Akkermansia-enriched gut is conceptually reminiscent of the SFB-driven Th17 program[34,35], in which dendritic-cell MHC-II presentation and commensal-specific TCR selection create a Th17-polarizing milieu that instructs adaptive effector differentiation. Akk seems to promote a polarizing milieu encouraging Th1 programming of CD4+ cells without evidence for IRBP-specific microbial antigen mimicry.

We did not attempt to identify the HuFl microbial mimic, as identifying it would lack translational relevance. The R161 TCR recognizes a mouse class II (I-A^r)-restricted epitope of IRBP. Human MHC class II molecules would almost certainly present a different epitope(s) from any given antigen than does mouse I-A^r, plus the epitope(s) would differ between individuals, given the heterogeneity of human MHC haplotypes. Moreover, whereas IRBP is a dominant retinal autoantigen in mice, human uveitis more commonly involves recall responses to arrestin[1]. Therefore, although the HuFl R161H sEAU model cannot reveal specific antigenic targets involved in human uveitis, it can reveal conserved mechanisms shared across species, such as the microbial interaction network identified in this study.

A key feature of this microbial network is the negative relationship between Akkermansia and Firmicutes, which links gut microbial composition to systemic inflammation. This antagonism likely arises from multiple, non-mutually exclusive mechanisms. Both taxa are dominant colonizers of the colon and may engage in direct niche competition and indirect interactions. Akkermansia promotes mucus degradation during gut inflammation[36,37]. The compromised mucus barrier would exacerbate inflammation and

oxidative stress[38], creating inhospitable conditions for obligate anaerobes like Firmicutes. Finally, while Akk antagonizes SCFA-producing Firmicutes, their SCFAs can in turn act to suppress Akkermansia growth and mucolytic activity[39].

All those interactions are reflected in the V/F ratio, which may serve as an indicator of inflammatory state and immune polarization across species, supporting its translational value. A similar “legacy” metric Firmicutes to Bacteroidetes (F/B ratio) has been used to indicate overall shifts in gut microbiome composition, but is now being phased out due to its inconsistent disease associations[40,41]. We propose that the V/F ratio is more specifically informative in autoimmune and inflammatory settings.

Of note, numerous studies report an association between uveitic diseases and gut inflammation. Uveitis is associated with an increased risk of Crohn’s (but not of UC)[42], and Crohn’s patients are more likely than UC patients to develop uveitis[43]. The findings are compatible with the notion that the V/F ratio increases under conditions where gut inflammation co-occurs with extraintestinal autoimmunity. The V/F ratio may also rise under Th1-dominant inflammatory conditions, as observed in our data. Our analyses reveal elevated V/F ratios not only in our patients with uveitis, but also in published datasets from patients with MS[25] and IBD[26]. Within IBD, increases in V/F were evident in Crohn’s disease (Th1-dominant[44-46]), but not in UC (Th2-like[47-49]).

Limitations of the study: The complexity of the Akkermansia–Firmicutes axis poses a major challenge to resolving microbial relationships at species and strain levels. Emerging approaches such as bacterial spatial transcriptomics[50] are not yet sufficiently developed to dissect mechanisms by which Akkermansia antagonizes SCFA-producing Firmicutes. That said, outcompetition could involve physical elimination via bacteriocins acting on SCFA producers[51]. In addition, the asynchronous nature of disease development in individual mice and the limited capacity of our GF R161H colony constrains the scale and breadth of experiments. Consequently, some types of mechanistic studies, including administering individual SCFAs to HuFI mice for functional validation, could not be accommodated.

In conclusion, our findings show that a complex microbial interaction network—rather than individual taxa—plays a central role in shaping the gut–eye axis. The Akkermansia–Firmicutes relationship likely represents a generalizable ecological principle in which microbial competition influences systemic immune balance and susceptibility to

autoimmunity and inflammation, and which extends across species. Future studies aimed at defining the mechanisms by which Akkermansia gains an advantage over SCFA-producing Firmicutes, may guide the development of microbiome-based interventions for autoimmune and inflammatory diseases that intersect with gut dysregulation.

METHODS

Mice. R161H mice on the B10.RIII background[10] were bred in-house and maintained under SPF conditions and fed standard facility chow *ad libitum*. GF and HuFl R161H mice were maintained in the gnotobiotic isolators. The animal study protocol (NEI-688) was approved by the NEI Institutional Animal Care and Use Committee.

Generation of gnotobiotic mice with human stool samples. Human stool samples of healthy volunteers were collected at Keio University according to the study protocol[52] approved by the Institutional Review Boards (approval number 20150075) and informed consent was obtained from each subject. Stool samples were suspended in 20% glycerol in PBS, snap frozen in liquid nitrogen and stored at -80°C. The U, V, and W stocks were thawed and gavaged into GF R161H mice and individual cohort lines were established in separate gnotobiotic isolators.

Evaluation of uveitis phenotype. Development of uveitis was monitored by fundoscopic observation via a binocular microscope of anesthetized mice at the indicated age. For histopathology, eyes were enucleated and fixed in 4% glutaraldehyde for 1 h and transferred to 10% formaldehyde for additional 24 h, embedded in methacrylate, and processed for H&E staining. Disease scores of fundoscopy and histology were assigned by a masked observer on a scale of 0–4, according to the criteria for EAU scoring described in detail elsewhere which are based on the number, size and type of lesions[53].

HuFl R161H fecal suspension preparation. Cecal and colonic contents from HuFl mice of varying disease severity were collected under sterile conditions and immediately transferred on ice to an anaerobic chamber (Coy Laboratory Products). Contents were filtered three times through a 70 μm cell strainer in 20% glycerol–PBS, and aliquoted to

prevent repeated freeze–thaw cycles. Each sample was prepared from either individual mice or pools of mice with the same disease severity. The baseline HuFl suspension for reconstitution experiments was prepared from two mice with low uveitis scores and validated by 16S sequencing to contain ~1% Akkermansia (ranges 1–8% in tested samples).

In vivo microbial enrichment by gnotobiotic reconstitution. *A. muciniphila* or *E. coli* were cultured in mucin-BHI media inside the anaerobic chamber or in LB media in the aerobic incubator, respectively. Microbial monoculture was prepared in advance and the first passage timed to reach the exponential growth phase immediately prior to oral gavage. On the day of gavage, GF R161H were transferred from the gnotobiotic isolators to sterile and static microisolator cages with a Reemay filter top. Using sterile techniques, these mice were examined by fundoscopy and assigned to experimental or control groups based on initial uveitis disease scores (<1), age (4-7 weeks) and sex. While mice were recovering from anesthesia, gavage material was prepared inside the anaerobic chamber for *A. muciniphila* or in the aerobic bacterial hood for *E. coli*, or sterile PBS, which in the "HuFl base model" was combined with the selected HuFl fecal suspension, so each mouse in the experimental group would receive an additional ~10^8 CFU of the microbe of interest in 200uL HuFl fecal suspension via oral gavage. Fecal sampling and fundoscopy scoring were performed on a weekly basis, and mice were handled under sterile protocols, with cages opened only inside a biosafety cabinet.

Fecal DNA extraction and quantification of microbes. Fecal pellets were collected from individual mice, immediately frozen on dry ice and stored at -80°C until bacterial DNA extraction in house as previously described[54] or by the NCI Genetics and Microbiome Core. Absolute abundance of bacteria in each fecal sample was assessed by quantitative polymerase chain reaction (qPCR) using Akkermansia or *E. coli* standard curves with Fast SYBR Green Supermix (Applied Biosystems, Waltham, MA, USA) and run on a QuantStudio™ 7 Pro Real-Time PCR System (Applied Biosystems). Specific primers for Akkermansia were Akk.mu3.Fwd (5'- GCGTAGGCTGTTTCGTAAGTCGTGT GTGAAAG -3') and Akk.mu3.Rvs (5'-GAGTGTTCCCGATATCTACGCATTTCA -3')[55], and for *E. coli* were Uni515F (5'- GTGCCAGCMGCCGCGGTAA -3') and Ent826R (5'-

GCCTCAAGGGCACAACCTCCAAG -3')[56]. Five ng of fecal DNA was amplified per 10 µL reaction with the following cycling conditions: initial denaturation at 95 °C for 20 sec, followed by 40 cycles of 95 °C for 3 sec and 63 °C for 30 sec. A melt-curve analysis was included at the end of each run to confirm amplification specificity. Bacterial counts (CFU) per 5 ng of DNA were extrapolated from fitted standard curves correlating Cq values with bacterial quantity.

16S rRNA gene sequencing and analyses. Fecal samples were processed at the NCI Genetics and Microbiome Core for 16S rRNA gene sequencing as detailed in prior work[54]. 16S amplicon sequence variants (ASV) were inferred with YAMS16 v1.7 (https://github.com/jhbadger/YAMS16), a pipeline running DADA2[57], and taxonomically classified using the SILVA reference database (release 138.1)[58]. Microbial diversity, differential abundance and multivariable association analyses were performed with phyloseq v1.42.0[59], MaAsLin2 v1.12.0[60], microViz v0.12.3[61] in R. Microbial association networks were analyzed with NetCoMi[62].

Shotgun metagenomic sequencing and analyses. Selected DNA samples were submitted to CosmosID, Inc. (Germantown, MD, USA) for shallow shotgun sequencing (3 million reads per sample). Specifically, DNA libraries were prepared using the Nextera XT DNA Library Preparation Kit (Illumina, Inc., San Diego, CA, USA) and IDT Unique Dual Indexes with total DNA input of 1 ng. Genomic DNA was fragmented using a proportional amount of Illumina Nextera XT fragmentation enzyme. Unique dual indexes were added to each sample followed by 12 cycles of PCR to construct libraries. DNA libraries were purified using AMpure magnetic Beads (Beckman Coulter, Inc., Brea, CA, USA) and eluted in QIAGEN EB buffer. DNA libraries were quantified using Qubit 4 fluorometer and Qubit™ dsDNA HS Assay Kit. Libraries were then sequenced on the Element AVITI platform 2x150 bp. JAMS v1.9.9[63] and HUMAnN v3.9[64] were used for taxonomic and functional profiling, and genes involved in metabolic pathways of the main SCFAs (acetate, butyrate and propionate) were identified based on InterPro, Gene Ontology and Pfam annotations, and those present in the uveitis datasets were compared between diseased and healthy groups.

Targeted metabolomics and cytokine quantification. Cecal and colonic contents (collectively referred to as “fecal contents”), eyes, and serum were collected from age-matched mice at harvest. Eyes were fixed for histological analysis as described above. Fecal and serum samples were snap-frozen on dry ice and stored at −80 °C. For metabolite profiling, at least 100 mg of fecal contents and 150 µL of serum per mouse were transferred to designated tubes and shipped on dry ice to Metabolon, Inc. (Morrisville, NC, USA) for absolute quantification of eight short-chain fatty acids (acetic, propionic, butyric, isobutyric, 2-methylbutyric, valeric, isovaleric, and hexanoic acids). Serum cytokine concentrations were measured using the Mouse Inflammation Panel (13-plex, LEGENDplex™, BioLegend, San Diego, CA, USA) according to the manufacturer’s instructions. Data were acquired on a CytoFlex LX flow cytometer (Beckman coulter) and analyzed with LEGENDplex Data Analysis Software (BioLegend) to quantify cytokine levels based on standard curves.

Tissue harvesting and flow cytometry analyses. Peripheral lymphoid tissues (submandibular lymph nodes, spleen, peripheral lymph nodes, mesenteric lymph nodes), and gut lamina propria from small intestine and colon were collected and prepared for single cell suspensions as described elsewhere[2]. Cells were stained at the dilution of 1:1000 with fluorochrome-conjugated antibodies (clones) from BD Biosciences, BioLegend or eBioscience/Thermo Fisher Scientific. Surface staining panel: FITC-TCR beta chain (H57-597), BB700-CD69 (H1.2F3), PE-CD62L (MEL-14), PE/Dazzle594 CD183/CXCR3 (CXCR3-173), PE/Cy7-CD199/CCR9 (CW-1.2), Alexa Fluor 700 CD8a (53-6.7), APC-eFluor 780-CD44 (IM7), Brilliant Violet (BV) 421-CD103 (2E7), BV510-CD45 (30-F11), BV650-CD4 (RM4-5), BV785-CD196/CCR6 (29-2L17), BUV496-CD3 (145-2C11). Intracellular staining panel: Alexa Fluor 488-IL-17F (9D3.1C8), PerCP/Cyanine5.5-T-bet (4B10), PE-RORgt (Q31-378) PE/Dazzle594-IL-10 (JES5-16E3), PE/Cy7-GM-CSF (MP1-22E9), APC-IL-22 (IL22JOP), Alexa Fluor 700-Foxp3 (FJK-16s), APC-eFluor 780-CD8a (53-6.7), BV421-IFN-g (XMG1.2), BV510-CD4 (RM4-5), BV650-IL-17A (TC11-18H10), BV786-CD44 (IM7), BUV496-CD3 (145-2C11). Dead cells were excluded by staining with ViaKrome 808 Fixable Viability Dye from Beckman Coulter. Fluorescence-activated cell sorting analyses were done using CytoFlex LX (Beckman coulter). FlowJo v10 (BD Biosciences) was used for data analyses.

In vitro activation assay on retina-specific T cells. IRBP-specific T cells were harvested from spleen and peripheral lymph nodes of *Tcra*$^{-/-}$ *Nr4a1*^{EGFP} (Nur77^{GFP}) R161H mice and were enriched for naïve CD4^{+} cells by negative selection using Mouse Streptavidin Rapidsphere Isolation Kit (EasySep, StemCell Technologies). The following biotin-conjugated anti-mouse antibodies (clones) from BioLegend, BD Biosciences were used at 1:250 dilutions: CD8 (53-6.7), CD11b (M1/70), CD11c (N418), CD16/32 (93), CD19 (6D5), CD24 (M1/69), CD25 (PC61), CD49b (DX5) CD69 (H1.2F3), CD45R/B220 (RA3-6B2), Ly-6G/Ly-6C (Gr1, RB-8C5), I-A/I-E (M5/114.15.2), NK1.1 (PK136), $\gamma\delta$TCR (GL3), Ter 119 (TER-119). CD11c^{+} dendritic cells were purified from spleen of WT B10.RIII mice as antigen-presenting cells using CD11c MicroBeads Ultrapure (Miltenyi Biotec). T cells and dendritic cells were co-cultured at a 4:1 ratio in the presence of heat-killed *A. muciniphila* (95°C for 5 min), heat-killed *E. coli* (60°C for 30 min), or bacteria-rich extracts from the gut content[2]. T cell activation was assessed after 22 h by flow cytometric analysis of CD69 and Nur77 expression.

5' single cell RNAseq sample processing. Cells from colon LP were labeled with TotalSeq C anti-mouse HashTags 1-10 (C0301-C0310, clones M1/42; 30-F11) and 14 cell surface antibodies from BioLegend at the dilution of 1:100. Cell surface anti-mouse antibodies: CD4 (DNA_ID C0001, clone RM4-5), CD8a (C0002, 53-6.7), Ly-6C (C0013, HK1.4), CD11b (C0014, M1/70), Ly-6G (C0015, 1A8), CD90.2 (C0075, 30-H12), CD19 (C0093, 6D5), CD11c (C0106, N418), F4/80 (C0114, BM8), I-A/I-E (C0117, M5/114.15.2), NK-1.1 (C0118, PK136), TCRβ chain (C0120, H57-597), TCR g/d (C0121, GL3), and CD3 (C0182, 17A2). Labeled cells were sorted for live CD45^{+} and CD4^{+} populations with PE anti-mouse CD45.2 (clone 104, BioLegend), eFluor^{TM} 450 anti-mouse CD4 (clone RM4-5, eBioscience) and 7-AAD (eBioscience) using FACSAria III/Fusion sorters (BD Biosciences). Post-sort viability exceeded 80%, and hash-tagged samples were pooled at equal ratios within each experimental group, combining CD45^{+} and CD4^{+} fractions at 1:1 ratio to enrich for CD4^{+} T cells. Pooled cells were resuspended in PBS with 0.04% BSA and loaded onto a 10x Genomics Chromium X instrument at 700–1200 cells/μL for single cell 5' gene expression and TCR profiling. Libraries were prepared using the Chromium Next GEM Single Cell 5' Reagent Kits v2

(Dual Index) following the manufacturer's protocol, and sequenced on NovaSeq 6000 platform (Illumina, Inc., San Diego, CA, USA).

Single cell RNAseq data analyses. Six mice (three from each group) were used for analyses. Sequencing data were processed with Cell Ranger v9.0.1 (10x Genomics) for demultiplexing and alignment to the Mus musculus reference (GRCm39, Genome Reference Consortium, 2024). Cell doublets were detected and removed using Scrublet v0.2.3[65]. Cells exhibiting high mitochondrial transcript content (≥ 5%) or abnormal gene counts (< 500 or > 8000) were excluded. Expression data were log-normalized and scaled using the Scanpy v1.11.0[66] in Python v3.10. Dimensionality reduction was performed using Principal Component Analysis (PCA) followed by Uniform Manifold Approximation and Projection (UMAP), and cell clusters were identified with the Leiden algorithm[67]. Cell type annotation was based on computational classification using SingleR v2.8.0[68] with mouse immune reference data from celldex::ImmGenData v1.16.0 in R v4.4, as well as the expression of canonical cell type marker genes, and validated by cell lineage–specific surface antibody. The expression of both Trav16 and Trbv5 in a CD4 T cell was the standard used to identify IRBP-specific T cells[10]. Seurat v5.1.0[69] was also used to generate object files for downstream application of CellChat[70] and SCENIC[71] in the R environment. CellChat was applied to infer changes in the strongest cell-cell interactions between Th1 cells and other cell types in the colon LP in Akk-rich mouse. SCENIC was used to reconstruct gene regulatory networks and to assess transcription factor activity at the single-cell level, enabling identification of Akkermansia-associated alterations in Th1 cell programming and lineage maintenance.

***NEI clinical samples and public human data*.** Stool samples were obtained from patients with autoimmune uveitis and healthy controls enrolled in a clinical cohort at the NEI, NIH. All participants provided written informed consent under the protocol approved by the Institutional Review Board (Protocol 13-EI-0072). A stratified cohort of treatment-naïve autoimmune uveitis was selected for in-depth gut microbial network analysis, representing primarily posterior- and pan-uveitis cases and ocular-restricted phenotypes such as idiopathic uveitis and birdshot chorioretinopathy. 16S rRNA gene and shotgun metagenomic sequencing of human fecal samples were performed by the Microbiome

Cores at the NCI and the Goodman-Luskin Microbiome Center (Los Angeles, CA, USA). Public microbiome data of IBD patients' stool are from PRJNA1198911[26], and that of MS patient stool from the International MS Microbiome Study (iMSMS)[25].

Statistical analyses. Statistical analyses were conducted with R v4.4, Python v3.10, and GraphPad Prism v10.5.0. Non-parametric tests such as Mann-Whitney U and Kruskal-Wallis tests were used for most comparisons between two or more groups. Group differences in multivariate community structure were evaluated by Permutational Multivariate Analysis of Variance (PERMANOVA). Pearson's or Spearman's rank correlation, as well as multivariable association (MaAsLin2 and equivalent methods) were used to assess associations between microbial features and disease or immune phenotypes. P-values were adjusted for multiple comparisons using the false discovery rate (FDR) where applicable, and statistical significance was indicated as follows: * $P < 0.05$, ** $P < 0.01$, *** $P < 0.001$, and **** $P < 0.0001$. Data in bar plots are presented as mean values ± SEMs.

Data availability. Raw microbiome sequencing data, including 16S rRNA gene amplicon and shotgun metagenomic sequencing reads from mouse samples and de-identified human samples, have been deposited in the NCBI Sequence Read Archive (SRA) under BioProject ID PRJNA1451962. Raw and processed single-cell RNA sequencing data have been deposited in the Gene Expression Omnibus (GEO) under accession number GSE327793.

Code availability. No custom code was developed for this study. All analyses were performed using publicly available software packages, and the specific versions and parameters used are described in the Methods section.

REFERENCES

1 Caspi, R. R. A look at autoimmunity and inflammation in the eye. *J Clin Invest* **120**, 3073-3083 (2010).

2 Horai, R. *et al.* Microbiota-Dependent Activation of an Autoreactive T Cell Receptor Provokes Autoimmunity in an Immunologically Privileged Site. *Immunity* **43**, 343-353 (2015).

3 Horai, R. & Caspi, R. R. Microbiome and Autoimmune Uveitis. *Front Immunol* **10**, 232 (2019).

4 Salvador, R., Zhang, A., Horai, R. & Caspi, R. R. Microbiota as Drivers and as Therapeutic Targets in Ocular and Tissue Specific Autoimmunity. *Front Cell Dev Biol* **8**, 606751 (2020).

5 White, Z. *et al.* Gut inflammation promotes microbiota-specific CD4 T cell-mediated neuroinflammation. *Nature* **643**, 509-518 (2025).

6 Lee, H. G. *et al.* Pathogenic function of bystander-activated memory-like CD4(+) T cells in autoimmune encephalomyelitis. *Nat Commun* **10**, 709 (2019).

7 Miller, S. D. *et al.* Persistent infection with Theiler's virus leads to CNS autoimmunity via epitope spreading. *Nat Med* **3**, 1133-1136 (1997).

8 Deeg, C. A., Amann, B., Raith, A. J. & Kaspers, B. Inter- and intramolecular epitope spreading in equine recurrent uveitis. *Invest Ophthalmol Vis Sci* **47**, 652-656 (2006).

9 Ji, Q., Perchellet, A. & Goverman, J. M. Viral infection triggers central nervous system autoimmunity via activation of CD8+ T cells expressing dual TCRs. *Nat Immunol* **11**, 628-634 (2010).

10 Horai, R. *et al.* Breakdown of immune privilege and spontaneous autoimmunity in mice expressing a transgenic T cell receptor specific for a retinal autoantigen. *J Autoimmun* **44**, 21-33 (2013).

11 Nakamura, Y. K. *et al.* Gut Microbial Alterations Associated With Protection From Autoimmune Uveitis. *Invest Ophthalmol Vis Sci* **57**, 3747-3758 (2016).

12 Shimizu, J. *et al.* Bifidobacteria Abundance-Featured Gut Microbiota Compositional Change in Patients with Behcet's Disease. *PLoS One* **11**, e0153746 (2016).

13 Huang, X. *et al.* Gut Microbiota Composition and Fecal Metabolic Phenotype in Patients With Acute Anterior Uveitis. *Invest Ophthalmol Vis Sci* **59**, 1523-1531 (2018).

14 Kalyana Chakravarthy, S. *et al.* Dysbiosis in the Gut Bacterial Microbiome of Patients with Uveitis, an Inflammatory Disease of the Eye. *Indian J Microbiol* **58**, 457-469 (2018).

15 Ye, Z. *et al.* A metagenomic study of the gut microbiome in Behcet's disease. *Microbiome* **6**, 135 (2018).

16 Ye, Z. *et al.* Altered gut microbiome composition in patients with Vogt-Koyanagi-Harada disease. *Gut Microbes* **11**, 539-555 (2020).

17 Steimle, A. *et al.* Gut microbial factors predict disease severity in a mouse model of multiple sclerosis. *Nat Microbiol* **9**, 2244-2261 (2024).

18 Luger, D. *et al.* Either a Th17 or a Th1 effector response can drive autoimmunity: conditions of disease induction affect dominant effector category. *J Exp Med* **205**, 799-810 (2008).

19 Damsker, J. M., Hansen, A. M. & Caspi, R. R. Th1 and Th17 cells: adversaries and collaborators. *Ann N Y Acad Sci* **1183**, 211-221 (2010).

20 Horai, R. & Caspi, R. R. Cytokines in autoimmune uveitis. *J Interferon Cytokine Res* **31**, 733-744 (2011).

21 Mann, E. R., Lam, Y. K. & Uhlig, H. H. Short-chain fatty acids: linking diet, the microbiome and immunity. *Nat Rev Immunol* **24**, 577-595 (2024).

22 Nakamura, Y. K. *et al.* Short chain fatty acids ameliorate immune-mediated uveitis partially by altering migration of lymphocytes from the intestine. *Sci Rep* **7**, 11745 (2017).

23 Chen, X. *et al.* Sodium butyrate regulates Th17/Treg cell balance to ameliorate uveitis via the Nrf2/HO-1 pathway. *Biochem Pharmacol* **142**, 111-119 (2017).

24 Louis, P. & Flint, H. J. Formation of propionate and butyrate by the human colonic microbiota. *Environ Microbiol* **19**, 29-41 (2017).

25 iMSMS Consortium. Gut microbiome of multiple sclerosis patients and paired household healthy controls reveal associations with disease risk and course. *Cell* **185**, 3467-3486 e3416 (2022).

26 Orejudo, M. *et al.* Exploration of fecal microbiota in newly diagnosed patients with inflammatory bowel disease using shotgun metagenomics. *Front Cell Infect Microbiol* **15**, 1595884 (2025).

27 Strober, W., Fuss, I. & Mannon, P. The fundamental basis of inflammatory bowel disease. *J Clin Invest* **117**, 514-521 (2007).

28 Guan, Q. A Comprehensive Review and Update on the Pathogenesis of Inflammatory Bowel Disease. *J Immunol Res* **2019**, 7247238 (2019).

29 Cani, P. D., Depommier, C., Derrien, M., Everard, A. & de Vos, W. M. Akkermansia muciniphila: paradigm for next-generation beneficial microorganisms. *Nat Rev Gastroenterol Hepatol* **19**, 625-637 (2022).

30 Cekanaviciute, E. *et al.* Gut bacteria from multiple sclerosis patients modulate human T cells and exacerbate symptoms in mouse models. *Proc Natl Acad Sci U S A* **114**, 10713-10718 (2017).

31 Berer, K. *et al.* Gut microbiota from multiple sclerosis patients enables spontaneous autoimmune encephalomyelitis in mice. *Proc Natl Acad Sci U S A* **114**, 10719-10724 (2017).

32 Jangi, S. *et al.* Alterations of the human gut microbiome in multiple sclerosis. *Nat Commun* **7**, 12015 (2016).

33 Ansaldo, E. *et al.* Akkermansia muciniphila induces intestinal adaptive immune responses during homeostasis. *Science* **364**, 1179-1184 (2019).

34 Goto, Y. *et al.* Segmented filamentous bacteria antigens presented by intestinal dendritic cells drive mucosal Th17 cell differentiation. *Immunity* **40**, 594-607 (2014).

35 Yang, Y. *et al.* Focused specificity of intestinal TH17 cells towards commensal bacterial antigens. *Nature* **510**, 152-156 (2014).

36 Desai, M. S. *et al.* A Dietary Fiber-Deprived Gut Microbiota Degrades the Colonic Mucus Barrier and Enhances Pathogen Susceptibility. *Cell* **167**, 1339-1353 e1321 (2016).

37 Tingler, A. M. & Engevik, M. A. Breaking down barriers: is intestinal mucus degradation by Akkermansia muciniphila beneficial or harmful? *Infect Immun* **93**, e0050324 (2025).

38 Sugihara, K. *et al.* Mucolytic bacteria license pathobionts to acquire host-derived nutrients during dietary nutrient restriction. *Cell Rep* **40**, 111093 (2022).

39 Schwabkey, Z. I. *et al.* Diet-derived metabolites and mucus link the gut microbiome to fever after cytotoxic cancer treatment. *Sci Transl Med* **14**, eabo3445 (2022).

40 Magne, F. *et al.* The Firmicutes/Bacteroidetes Ratio: A Relevant Marker of Gut Dysbiosis in Obese Patients? *Nutrients* **12** (2020).

41 Walters, W. A., Xu, Z. & Knight, R. Meta-analyses of human gut microbes associated with obesity and IBD. *FEBS Lett* **588**, 4223-4233 (2014).

42 Lo, T. C., Chen, Y. Y. & Chen, H. H. Risk of inflammatory bowel disease in uveitis patients: a population-based cohort study. *Eye (Lond)* **36**, 1288-1293 (2022).

43 Lin, H. *et al.* Differences in the prevalence of uveitis between Crohn's disease and ulcerative colitis: A systematic review and meta-analysis. *Acta Ophthalmol* **102**, e485-e492 (2024).

44 Bouma, G. & Strober, W. The immunological and genetic basis of inflammatory bowel disease. *Nat Rev Immunol* **3**, 521-533 (2003).

45 Fuss, I. J. *et al.* Disparate CD4+ lamina propria (LP) lymphokine secretion profiles in inflammatory bowel disease. Crohn's disease LP cells manifest increased secretion of IFN-

gamma, whereas ulcerative colitis LP cells manifest increased secretion of IL-5. *J Immunol* **157**, 1261-1270 (1996).

46 Parronchi, P. *et al.* Type 1 T-helper cell predominance and interleukin-12 expression in the gut of patients with Crohn's disease. *Am J Pathol* **150**, 823-832 (1997).

47 Fuss, I. J. *et al.* Nonclassical CD1d-restricted NK T cells that produce IL-13 characterize an atypical Th2 response in ulcerative colitis. *J Clin Invest* **113**, 1490-1497 (2004).

48 Heller, F. *et al.* Interleukin-13 is the key effector Th2 cytokine in ulcerative colitis that affects epithelial tight junctions, apoptosis, and cell restitution. *Gastroenterology* **129**, 550-564 (2005).

49 Strober, W. & Fuss, I. J. Proinflammatory cytokines in the pathogenesis of inflammatory bowel diseases. *Gastroenterology* **140**, 1756-1767 (2011).

50 Sarfatis, A., Wang, Y., Twumasi-Ankrah, N. & Moffitt, J. R. Highly multiplexed spatial transcriptomics in bacteria. *Science* **387**, eadr0932 (2025).

51 Montgomery, T. L. *et al.* Lactobacillaceae differentially impact butyrate-producing gut microbiota to drive CNS autoimmunity. *Gut Microbes* **16**, 2418415 (2024).

52 Tanoue, T. *et al.* A defined commensal consortium elicits CD8 T cells and anti-cancer immunity. *Nature* **565**, 600-605 (2019).

53 Horai, R. & Caspi, R. R. in *Animal Models for Retinal Diseases. Neuromethods.* Vol. 46 207-225 (SpringerLink, 2010).

54 Salvador, R. *et al.* Too Much of a Good Thing: Extended Duration of Gut Microbiota Depletion Reverses Protection From Experimental Autoimmune Uveitis. *Invest Ophthalmol Vis Sci* **64**, 43 (2023).

55 Goux, H. J., Chavan, D., Crum, M., Kourentzi, K. & Willson, R. C. Akkermansia muciniphila as a Model Case for the Development of an Improved Quantitative RPA Microbiome Assay. *Front Cell Infect Microbiol* **8**, 237 (2018).

56 Barman, M. *et al.* Enteric salmonellosis disrupts the microbial ecology of the murine gastrointestinal tract. *Infect Immun* **76**, 907-915 (2008).

57 Callahan, B. J. *et al.* DADA2: High-resolution sample inference from Illumina amplicon data. *Nat Methods* **13**, 581-583 (2016).

58 Quast, C. *et al.* The SILVA ribosomal RNA gene database project: improved data processing and web-based tools. *Nucleic Acids Res* **41**, D590-596 (2013).

59 McMurdie, P. J. & Holmes, S. phyloseq: an R package for reproducible interactive analysis and graphics of microbiome census data. *PLoS One* **8**, e61217 (2013).

60 Mallick, H. *et al.* Multivariable association discovery in population-scale meta-omics studies. *PLoS Comput Biol* **17**, e1009442 (2021).

61 Barnett, D. J. M., Arts, I. C. W. & Penders, J. microViz: an R package for microbiome data visualization and statistics. *J Open Source Software* **6** 3201 (2021).

62 Peschel, S., Muller, C. L., von Mutius, E., Boulesteix, A. L. & Depner, M. NetCoMi: network construction and comparison for microbiome data in R. *Brief Bioinform* **22** (2021).

63 McCulloch, J. A. *et al.* JAMS - A framework for the taxonomic and functional exploration of microbiological genomic data. *bioRxiv* (2023).

64 Beghini, F. *et al.* Integrating taxonomic, functional, and strain-level profiling of diverse microbial communities with bioBakery 3. *Elife* **10** (2021).

65 Wolock, S. L., Lopez, R. & Klein, A. M. Scrublet: Computational Identification of Cell Doublets in Single-Cell Transcriptomic Data. *Cell Syst* **8**, 281-291 e289 (2019).

66 Wolf, F. A., Angerer, P. & Theis, F. J. SCANPY: large-scale single-cell gene expression data analysis. *Genome Biol* **19**, 15 (2018).

67 Traag, V. A., Waltman, L. & van Eck, N. J. From Louvain to Leiden: guaranteeing well-connected communities. *Sci Rep* **9**, 5233 (2019).

68 Aran, D. *et al.* Reference-based analysis of lung single-cell sequencing reveals a transitional profibrotic macrophage. *Nat Immunol* **20**, 163-172 (2019).

69 Hao, Y. *et al.* Dictionary learning for integrative, multimodal and scalable single-cell analysis. *Nat Biotechnol* **42**, 293-304 (2024).

70 Jin, S. *et al.* Inference and analysis of cell-cell communication using CellChat. *Nat Commun* **12**, 1088 (2021).

71 Aibar, S. *et al.* SCENIC: single-cell regulatory network inference and clustering. *Nat Methods* **14**, 1083-1086 (2017).

Author contributions

A.Z., R.H. and R.R.C. conceived and designed the study. R.R.C and R.H. supervised the project. A.Z., R.H., Y.J., A.G., S.A., and C.E.M. performed experiments and collected data. A.Z., J.H.B., Z.W., G.S., and V.N. performed computational analyses. S.H., H.N.S., J.W.L. and K.H. provided human microbiome samples, and S.K. and H.N.S. contributed to clinical interpretation. X.X., M.J.M., Z.P., B.X. provided experimental input and technical assistance. R.P. and N.M. provided technical expertise in bacteriology. J.H.B., Z.W., J.A.M., J.P.J. and C.O. contributed analytical tools, resources and expertise. A.Z. and R.H. analyzed and interpreted data and prepared figures. A.Z., R.H. and R.R.C. wrote and finalized the manuscript. All authors discussed the results, reviewed, and approved the final manuscript.

Acknowledgments

We are grateful to NEI and NHLBI Flow Cytometry Cores, NEI Histology and Genetic Engineering Cores, Ms. Wuxing Yuan, Dr. Shah Rashed and members of NCI Microbiome Core, UCLA Goodman-Luskin Microbiome Center Microbiome Core, and all members of the Caspi Lab for their invaluable experimental assistance. We extend special thanks to Dr. Katsuko Sudo (Tokyo Medical University, Japan), Mr. Hirofumi Kobayashi and staff at Sankyo Labo Service Corporation, Inc. (Japan), as well as the gnotobiotic management team from NEI Veterinary Research and Resources Section for their expert support and guidance in GF and gnotobiotic colony maintenance. We also thank Dr. Eduard Ansaldo (NIAID) for sharing protocols for Akkermansia culture, Dr. Kikuji Itoh (Japan SLC, Inc.), Dr. Koji Atarashi and members of the Honda Lab for providing experimental advice. Finally, we acknowledge Dr. Geoffrey A. Mueller and staff at NIEHS Nuclear Magnetic Resonance Group for their generous assistance with metabolomics, and Drs. Kelsey Wheeler, Daniel Sellers, and Reuben Allen (Massachusetts Institute of Technology) for their insightful discussions and critical feedback. This study was supported by NIH/NEI Intramural funding, Project Number EY000184.

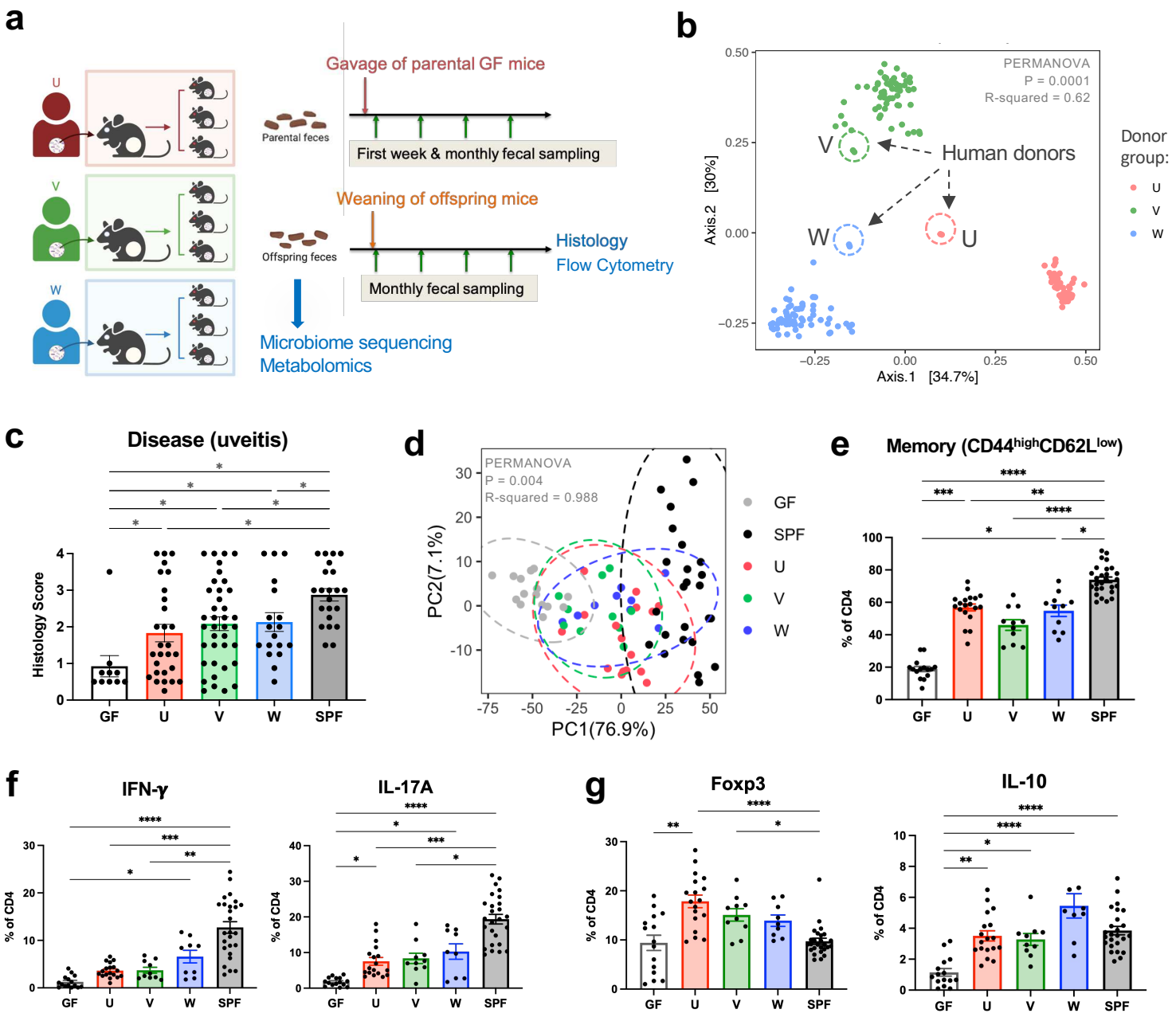


Fig. 1 | Human gut commensals support development of spontaneous experimental autoimmune uveitis (sEAU). a, Schematic representation of human fecal microbiota transfer experiments and data collection. **b**, Beta diversity based on Bray–Curtis dissimilarity showing differences in fecal microbiome composition between recipient groups U (n = 50), V (n = 59), W (n = 64). Encircled with dashed lines are the respective human donor (original) fecal samples. **c**, Disease scores (histology) of age-matched R161H mice (4-5 months old) from human flora (U, V, W, n = 28, 38, 18), SPF (n = 22) and GF (n = 10) groups (Kruskal–Wallis test between mouse recipient groups, p = 0.0002). **d**, Immunological clusters of CD4 T cells from colon lamina propria (LP) by the microbiome groups. PCA analysis performed on immune signature matrix by frequencies of CD4 T cells expressing each cell surface or intracellular marker (see **Extended Data Fig. 1e**). **e**–**g**, Frequencies of memory ($CD44^{high}CD62L^{low}$, **e**), IFN-γ- or IL-17A-producing (**f**), and regulatory (Foxp3-positive or IL-10-producing, **g**) CD4 T cells in colon LP of HuFl, SPF and GF R161H mice. **d**–**g**, Compiled data from 12 experiments, n = 15, 19, 11, 11, 27 for GF, U, V, W and SPF, respectively. Kruskal–Wallis tests show p < 0.0001 (**e**–**g**). P-values adjusted for post hoc multiple comparisons are displayed as asterisks. *P < 0.05, **P < 0.01, ***P < 0.001, ****P < 0.0001, and bar plots showing mean values ± SEMs (**c**, **e**–**g**).

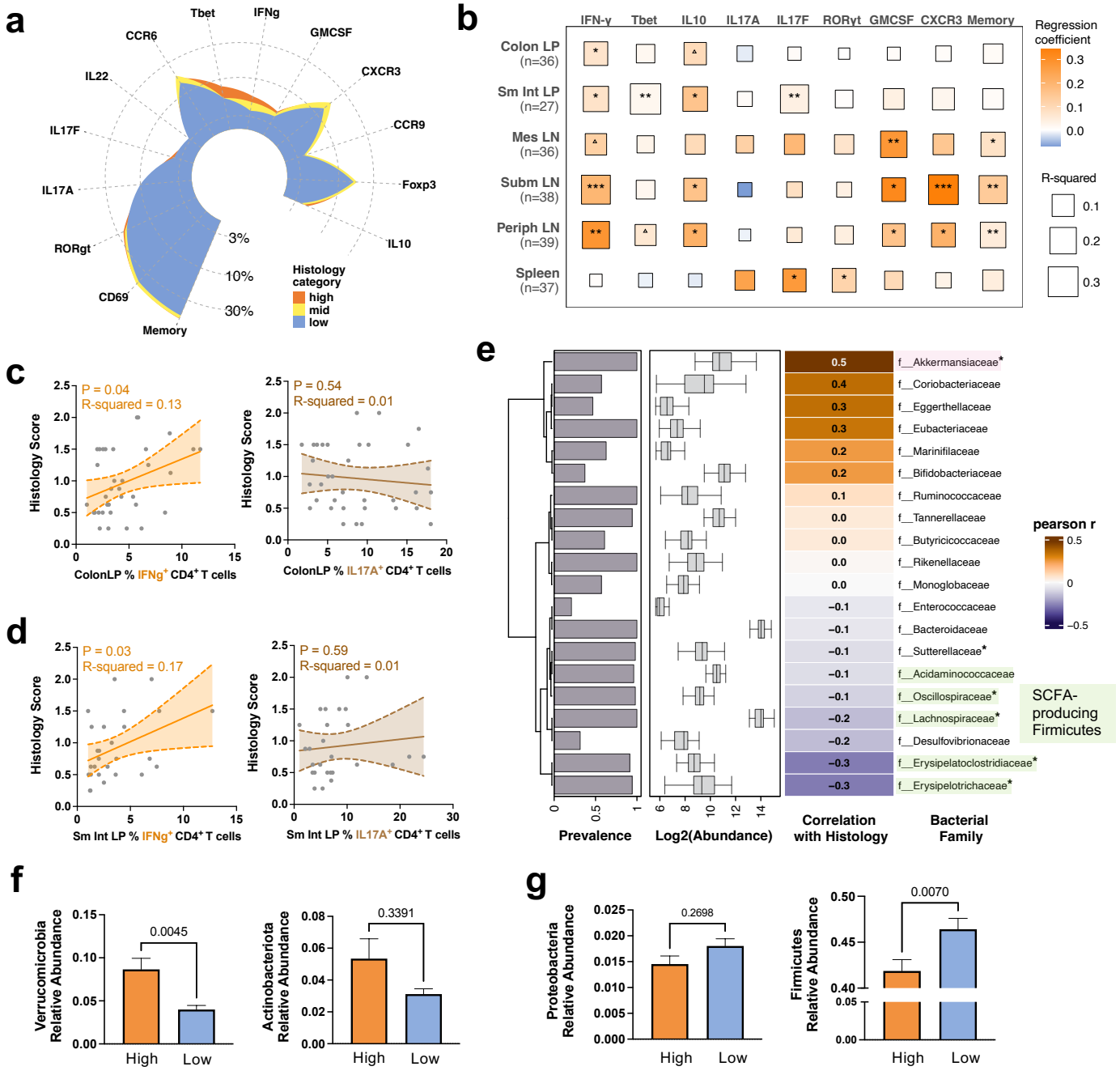


Fig. 2 | Human flora (HuFl) sEAU tracks with a dominant Th1 phenotype and abundance of Akkermansia (Verrucomicrobia). a, Mean relative frequency of colon LP CD4 T cells of each cell surface or intracellular marker arranged in a circular plot, colored by histology category: high (score ≥ 1.5, n = 10), mid (0.75 < score < 1.5, n = 8), low (score ≤ 0.75, n = 17). **b**, Correlational heatmap of histology scores with relative frequencies of each cell surface or intracellular marker in CD4 T cells across six tissue sites. LP, lamina propria; LN, lymph nodes; Sm Int, small intestine; Mes, mesenteric; Subm, submandibular; Periph, peripheral. $^{\Delta}0.05 < P < 0.08$, *P < 0.05, **P < 0.01, ***P < 0.001, modeled by simple linear regression. **c**–**d**, Representative trend lines with 95% confidence interval (shaded area) show that disease scores of HuFl mice are positively associated with IFN-γ-producing, but not IL-17A-producing, CD4 T cells, in colon LP (**c**) and small intestine LP (**d**). Data in **a**–**d** are aggregated from 8 experiments (UVW combined, sample sizes ranged from n = 27 to 39 across tissues following quality filtering). **e**, Correlational heatmap showing major fecal bacterial taxa (out of top 20 most abundant families) that correlate with disease scores in adult HuFl R161H (UVW combined, n = 105). P-values assessed after FDR (false discovery rate) correction following Pearson correlation. *P < 0.05. **f**–**g**, More Verrucomicrobia (**f**), and fewer Firmicutes (**g**) are present in the gut of HuFl mice with high disease scores. Sample sizes are n = 36 and 43 for high and low histology categories, respectively. Data in bar plots are presented as mean values ± SEMs, and P-values from Mann-Whitney U tests are shown in plots.

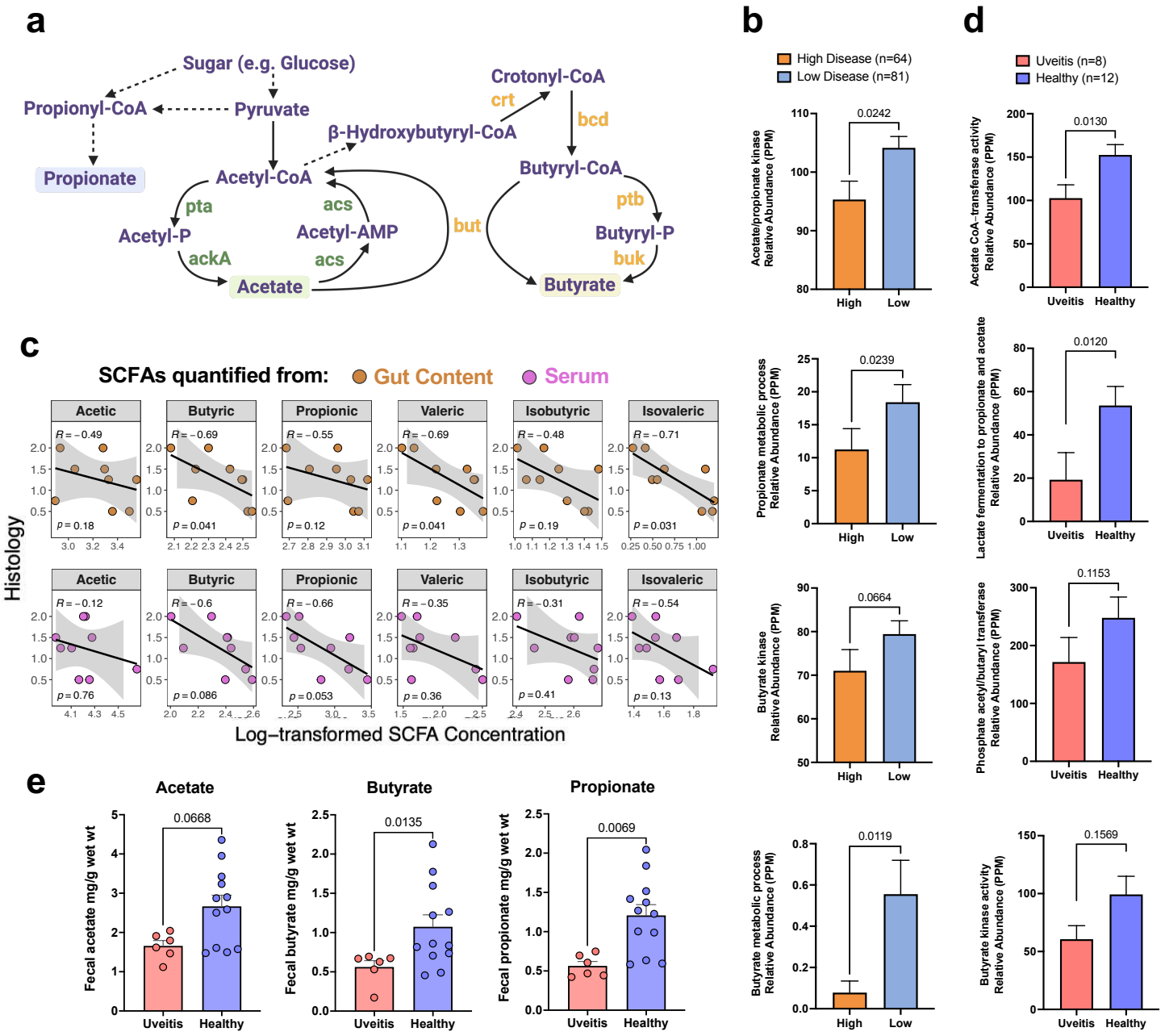


Fig. 3 | SCFA signatures are enriched in low disease HuFl mice or healthy subjects. a, A simplified pathway map highlighting functional genes involved in the main SCFA synthesis and metabolism. Dashed arrows indicate hidden intermediate steps. Abbreviations of enzyme symbols: pta, Phosphotransacetylase; ackA, Acetate kinase; acs, Acetyl-CoA synthetase; but, Butyryl-CoA:acetate CoA-transferase; ptb, Phosphate butyryltransferase; buk, Butyrate kinase; crt, Crotonase; bcd, Butyryl-CoA dehydrogenase. **b**, Enzymes in SCFA pathways (annotated with InterPro and Gene Ontology databases) are enriched in HuFl mouse gut with low histology scores (UVW combined, weanling and adult samples included). PPM, parts per million, a measure of relative abundance based on normalized base count for each feature in a metagenomic sample. **c**, Spearman correlation (visualized with a linear trend line) showing higher disease scores associated with lower SCFA concentrations both locally (in gut content) and systemically (in serum) in representative cohort U mice (n = 9). **d**, Enzymes in SCFA pathways (annotated with Gene Ontology and Pfam databases) are enriched in fecal samples from healthy humans compared to those from treatment-naïve uveitis patients, from a cohort of autoimmune uveitis (ocular-restricted, including idiopathic uveitis, VKH/SO and BCR). Sex, age, race and diet are comparably represented in patient and control groups. Normalized gene abundance is reported in PPM. **e**, SCFA levels from uveitis patients and healthy controls (same cohort as in **d,** but n = 6 available from the patient group). For **b, d** & **e**, Data are presented as mean values ± SEMs. Statistical significance was determined by Mann-Whitney U test.

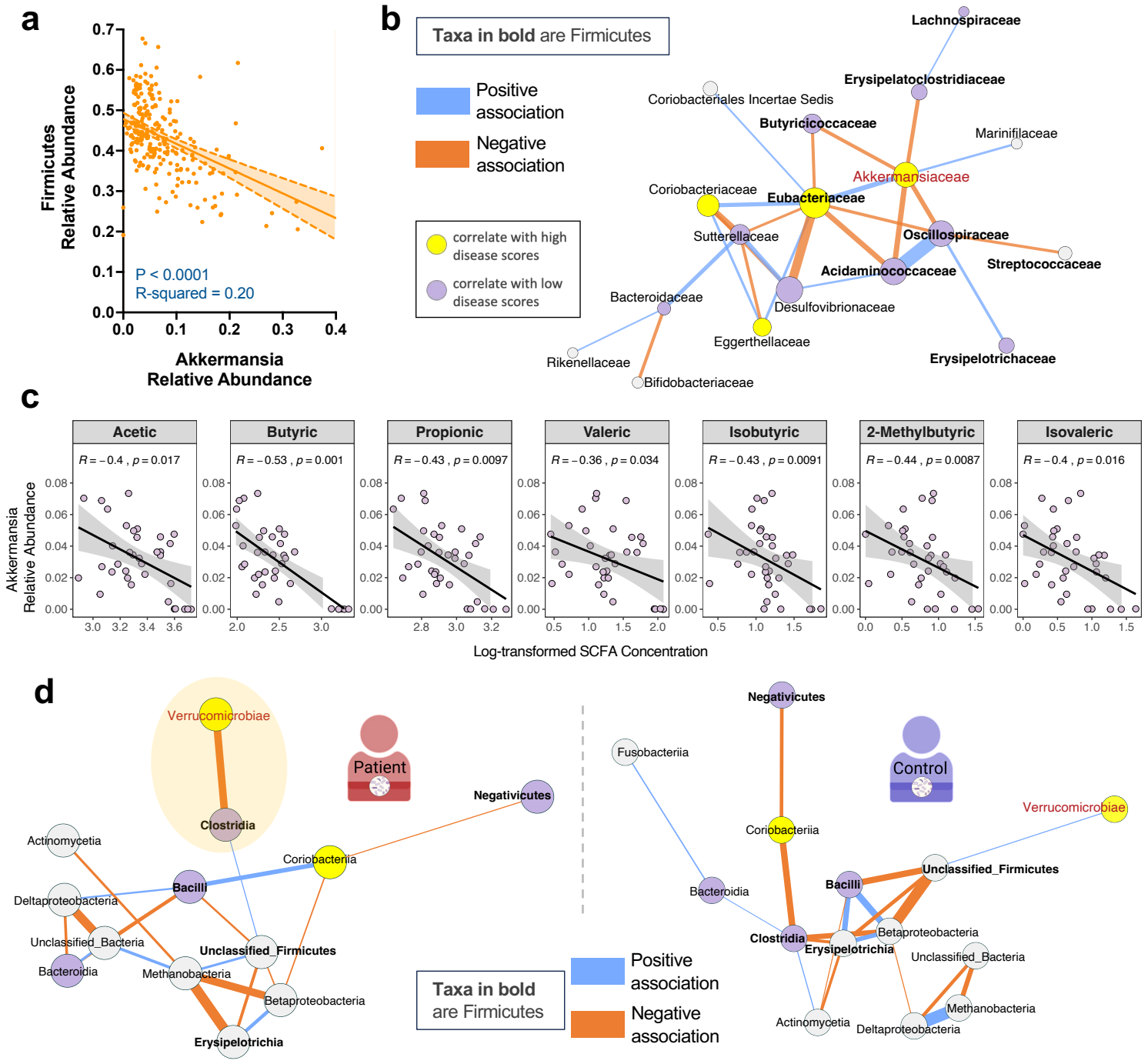


Fig. 4 | Akkermansia negatively correlates with Firmicutes in both sEAU and clinical uveitis. a, Simple linear regression showing a negative correlation of microbial relative abundance between Akkermansia (equivalent to Verrucomicrobia in this dataset) and Firmicutes in HuFl R161H mice (n = 234, UVW combined, weanling and adult samples included). **b**, Fecal bacterial association network exemplified in HuFl cohort V (n = 79, weanling and adult samples included). Network constructed at the taxonomic level of the bacterial family. Correlations with a threshold of Pearson r > 0.5 were transformed into dissimilarities via the "unsigned" distance metric, on which edge weights (strength of correlations) are based. Blue edges correspond to positive associations and orange edges to negative ones. Yellow and purple nodes represent taxa enriched in high *vs.* low disease categories, with Firmicutes labeled as bolded taxon names. Bigger nodes are more influential in the network (higher eigenvector centrality). **c**, Spearman correlation (visualized with a linear trend line) showing a negative association between relative Akkermansia abundance and SCFA concentrations in R161H gut (n = 35, UVW and SPF combined). Akkermansia was selected following multivariable association between SCFA concentrations and microbial features using MaAsLin2. **d**, Class level association networks in treatment-naïve uveitis patients (left, n = 8) and healthy controls (right , n = 12) from the same cohort of autoimmune uveitis. Correlations with a threshold of Pearson r > 0.3 are shown. Node and edge color schemes same as in **b**. Shaded ellipse in the patient network highlights the negative correlation between Verrucomicrobiae (Akkermansia) and Clostridia (Firmicutes), and this relationship is absent from the healthy human gut.

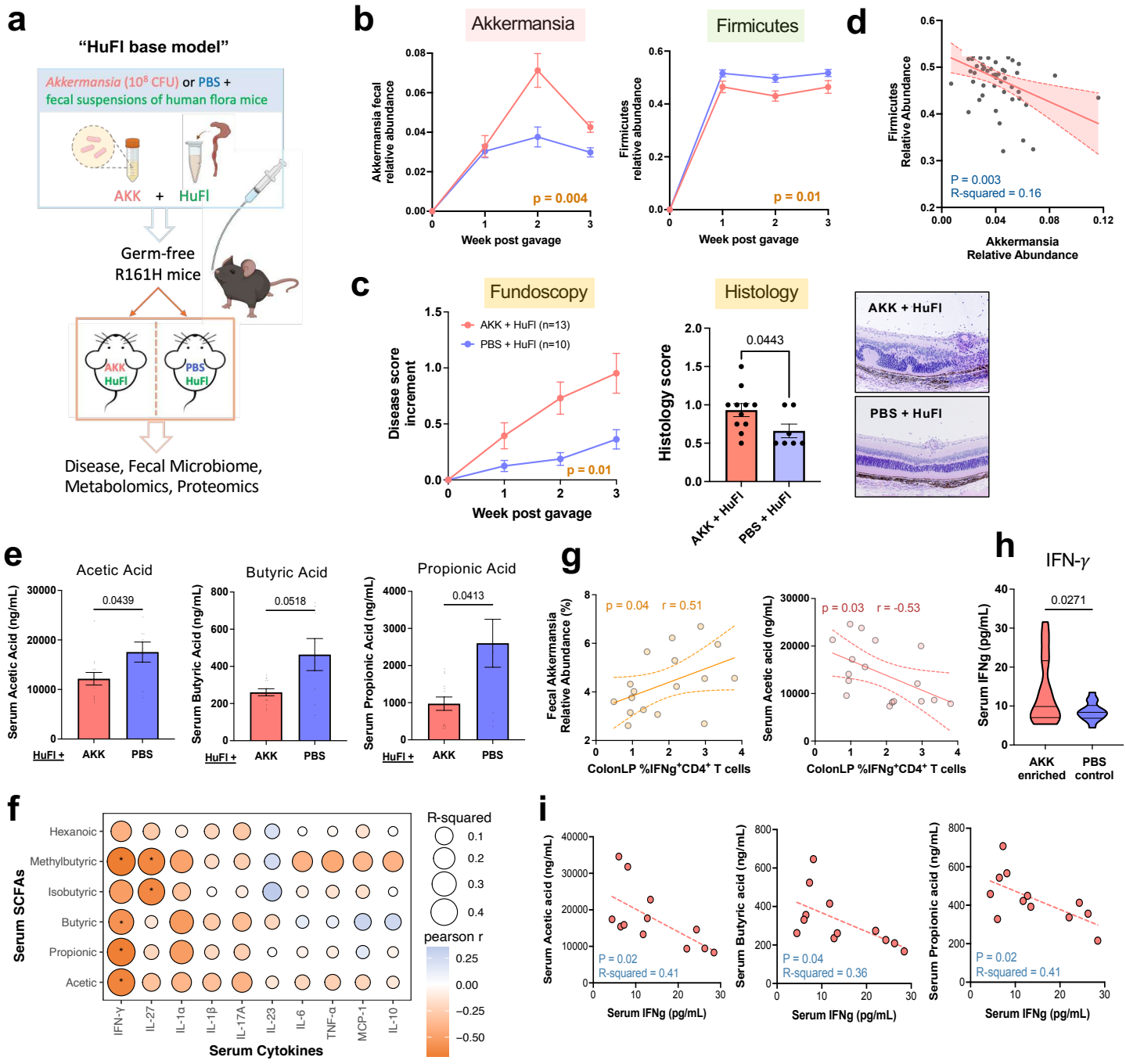


Fig. 5 | Akkermansia promotes uveitis by outcompeting SCFA producers and decreasing circulating SCFA levels. **a**, Study design of microbe reconstitution experiments. Previously GF R161H mice gavaged with a baseline human gut microbiota suspension (HuFl) plus *A. muciniphila* culture (AKK, 10^8 CFU) or sterile PBS. **b**, Relative abundance of Akkermansia and Firmicutes in feces from one representative of 3 experiments (n = 7 and 6 for Akk-rich and control, respectively). **c**, Left: Fundoscopy score increments from starting disease scores, combined from three experiments. Right: Histology scores and example images from 2 out of 3 experiments (n = 11 and 7 for Akk-rich and control, respectively). Mean values ± SEM. P-value determined by Welch-corrected t test. **d**, A negative correlation of relative abundance between Akkermansia and Firmicutes (n = 52, AKK and PBS groups combined, multiple time points included) by simple linear regression. **e**, Serum concentrations of main SCFAs are significantly lower in Akk-rich (n = 13) mice than in PBS controls (n = 10). Serum harvested 3 – 4 weeks post gavage, three experiments combined. **f**, Correlational heatmap of SCFA levels with cytokine concentrations in serum of engrafted mice. *P < 0.05, modeled by simple linear regression as well as Pearson correlation. **g**, Spearman correlation (visualized with a linear trend line) showing Akkermansia relative abundance associated positively, and serum acetic acid associated negatively, with the frequency of IFN-γ-producing CD4 T cells in colonic LP. **h**, Akk-enriched (n = 18) mice had higher serum IFN-γ concentrations compared to PBS control mice (n = 14), five experiments combined, of which two experiments used the minimal flora model. **i**, Representative trend lines show that main SCFA concentrations are negatively associated with IFN-γ levels in serum. Data in **g, i** are from 2 experiments (n = 12) using the minimal flora model.

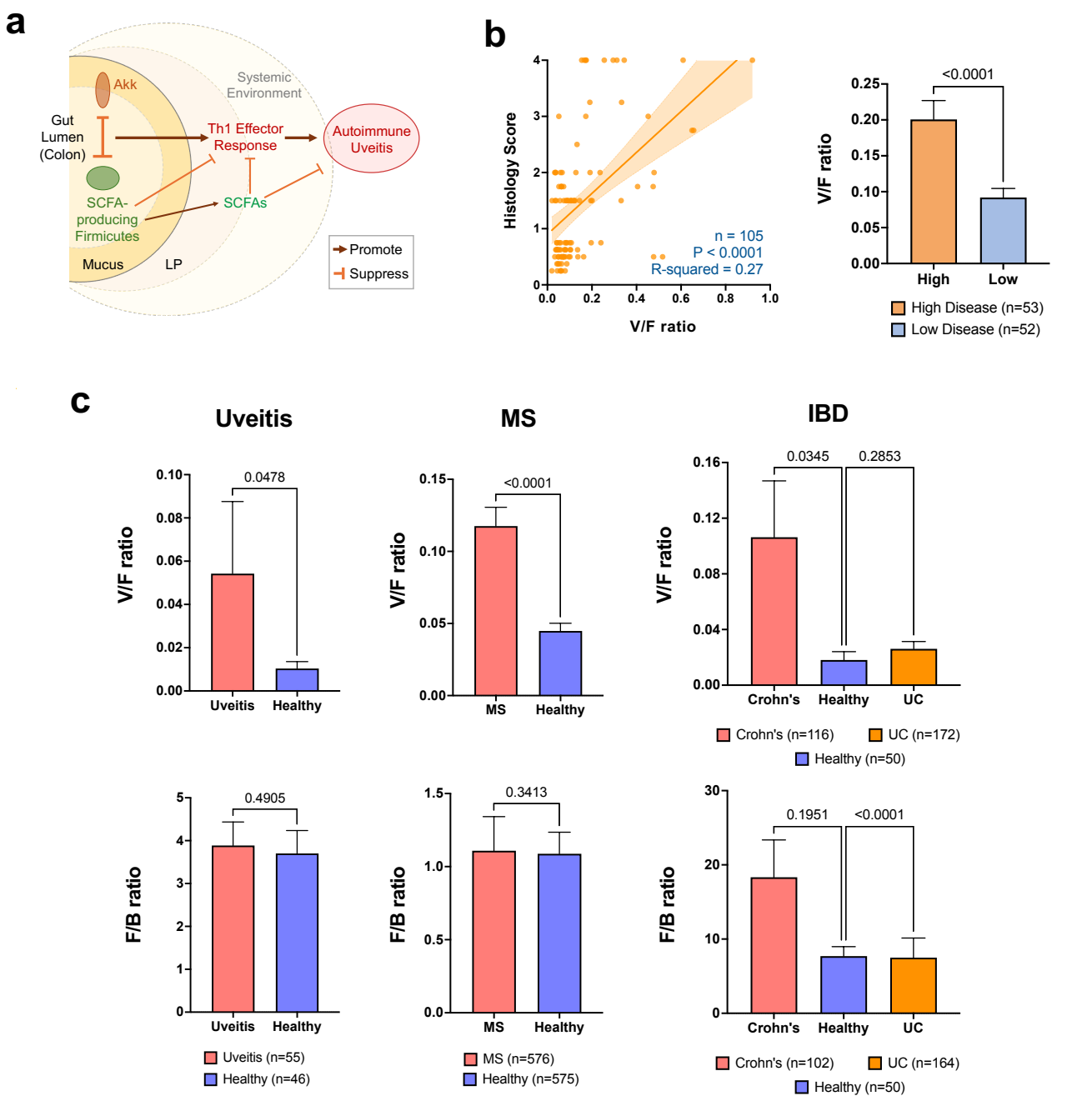
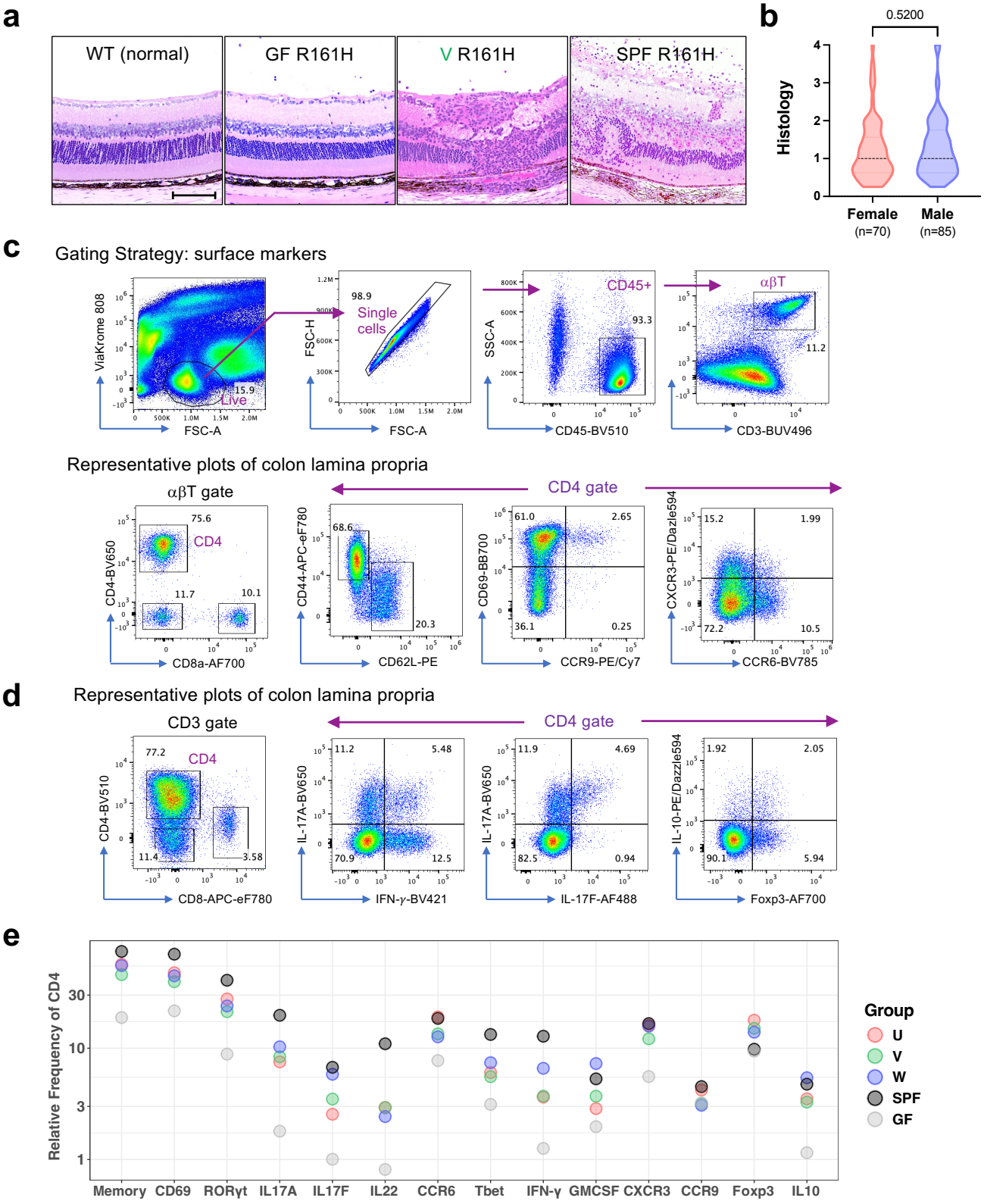
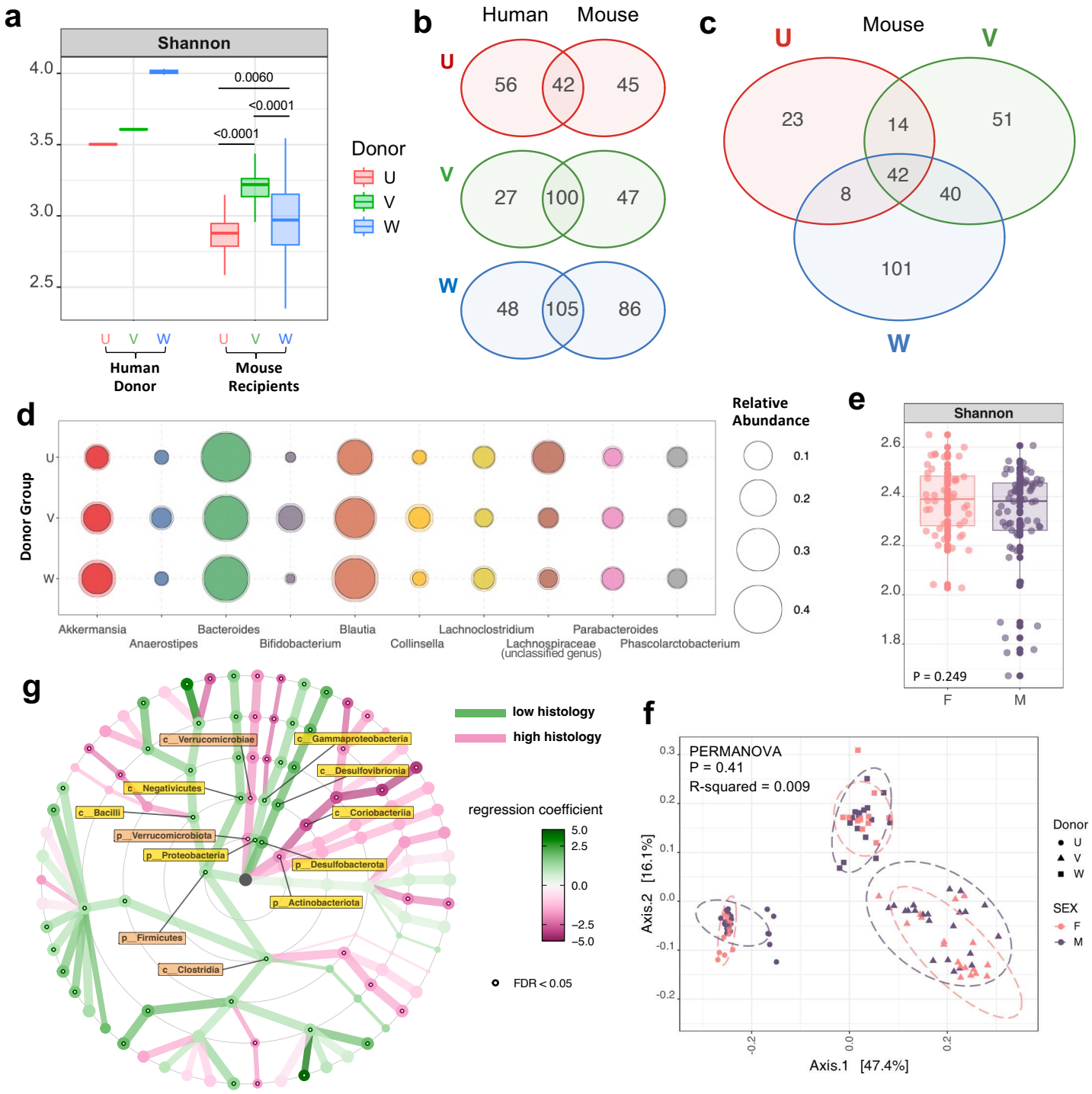


Fig. 6. **The inverse relationship between Verrucomicrobia and Firmicutes extends to clinical uveitis, multiple sclerosis (MS) and Crohn's disease. a**, Graphical summary of the working model. **b**, A positive correlation between V/F (Verrucomicrobia/Firmicutes) ratios and histology scores of HuFl mice by simple linear regression, and V/F ratios compared between high and low disease of HuFl mice. **c**, V/F and F/B (Firmicutes/ Bacteroidetes) ratios compared between patients from uveitis, MS and IBD and their respective healthy controls. Analyzed datasets of MS and IBD (Crohn's disease and UC) and healthy controls were from public sources. Uveitis and MS cohorts included those established on treatment. For F/B ratio in the IBD cohort, samples with <0.1% relative abundance of either Bacteroidetes or Firmicutes were removed from the analysis. Data are presented as mean values ± SEM. Statistical significance was determined by Mann-Whitney U test (one-tailed analysis was applied for uveitis and MS) and Kruskal–Wallis test with P-values adjusted for post hoc multiple comparisons (for IBD).

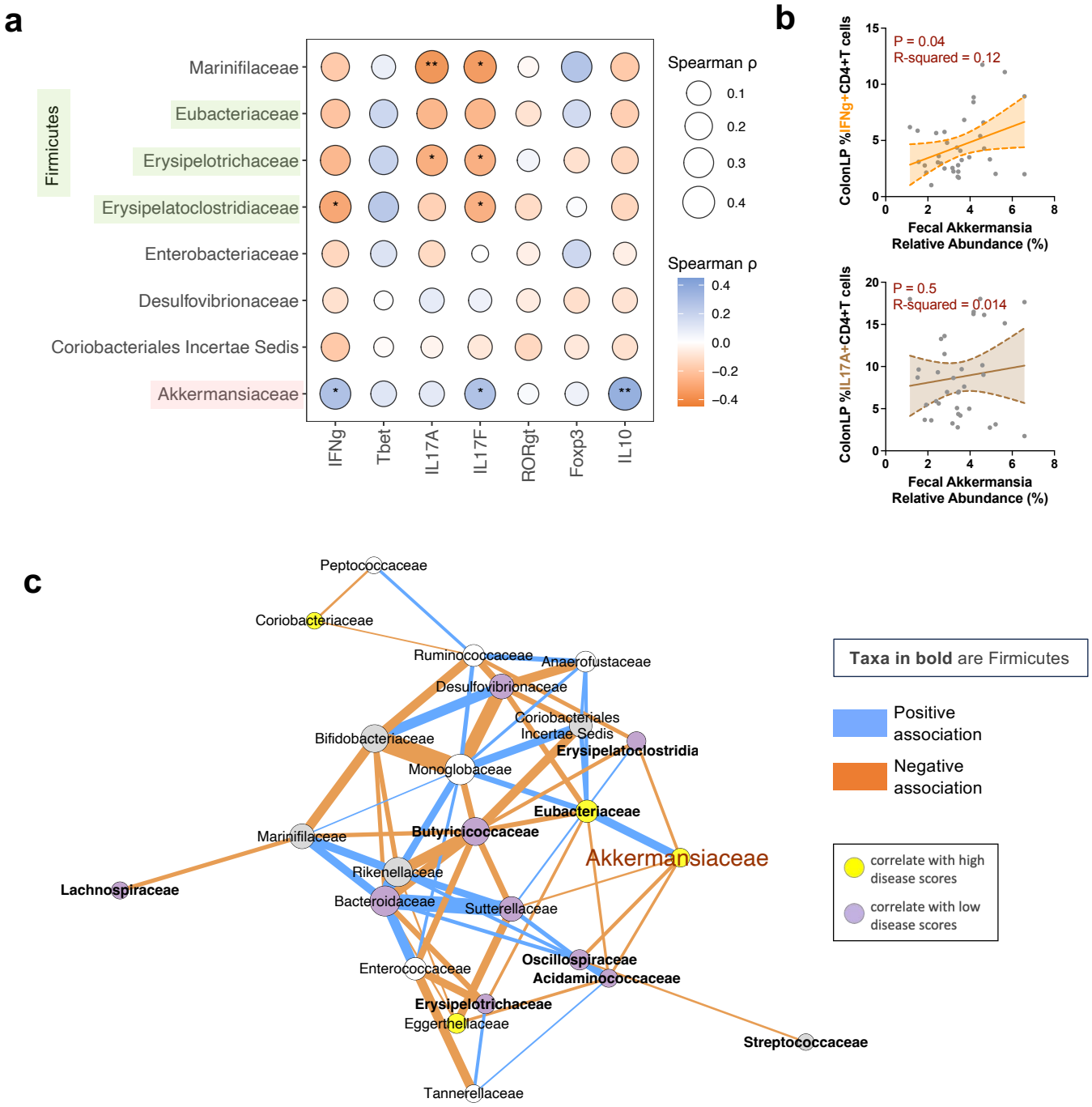
EXTENDED DATA



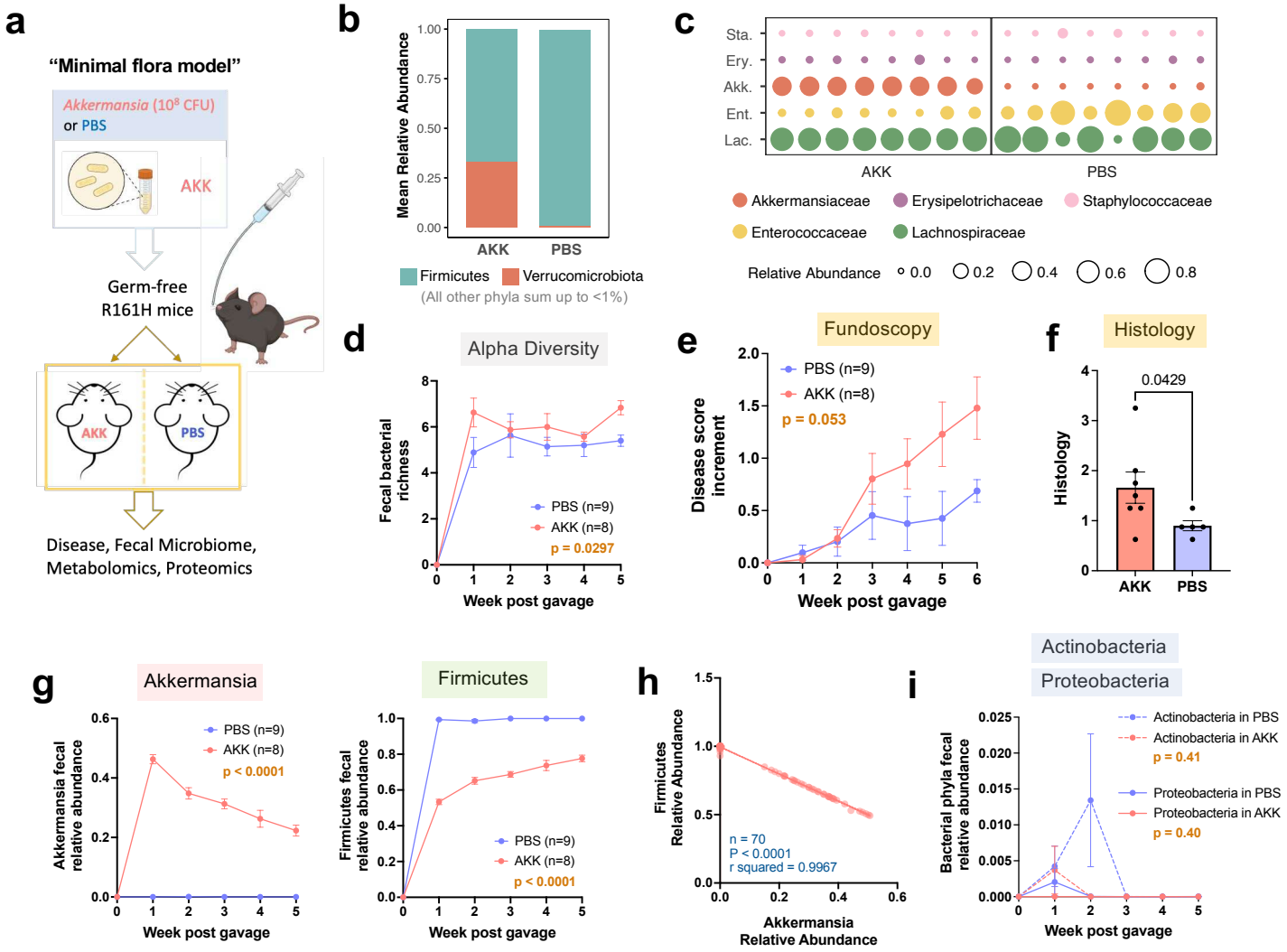
Extended Data Fig. 1 | Disease and CD4 T cell phenotypes of HuFl R161H. a, Representative retinal histology images contrasted between WT (normal retina) and R161H (GF, HuFl-V and SPF). The scale bar in the WT image shows 100 µm. **b**, Histology scores are comparable between female and male HuFl R161H mice at ages of 7-11 weeks old. Data combined from UVW cohorts (Mann-Whitney U test, p = 0.52). **c**, Gating strategy and representative flow cytometry plots of the surface markers from colon LP. **d**, Representative flow cytometry plots of the intracellular markers from colon LP. **e**, Mean relative frequency of each cell surface or intracellular marker of colon LP CD4 T cells, differentially colored by the microbiome groups.



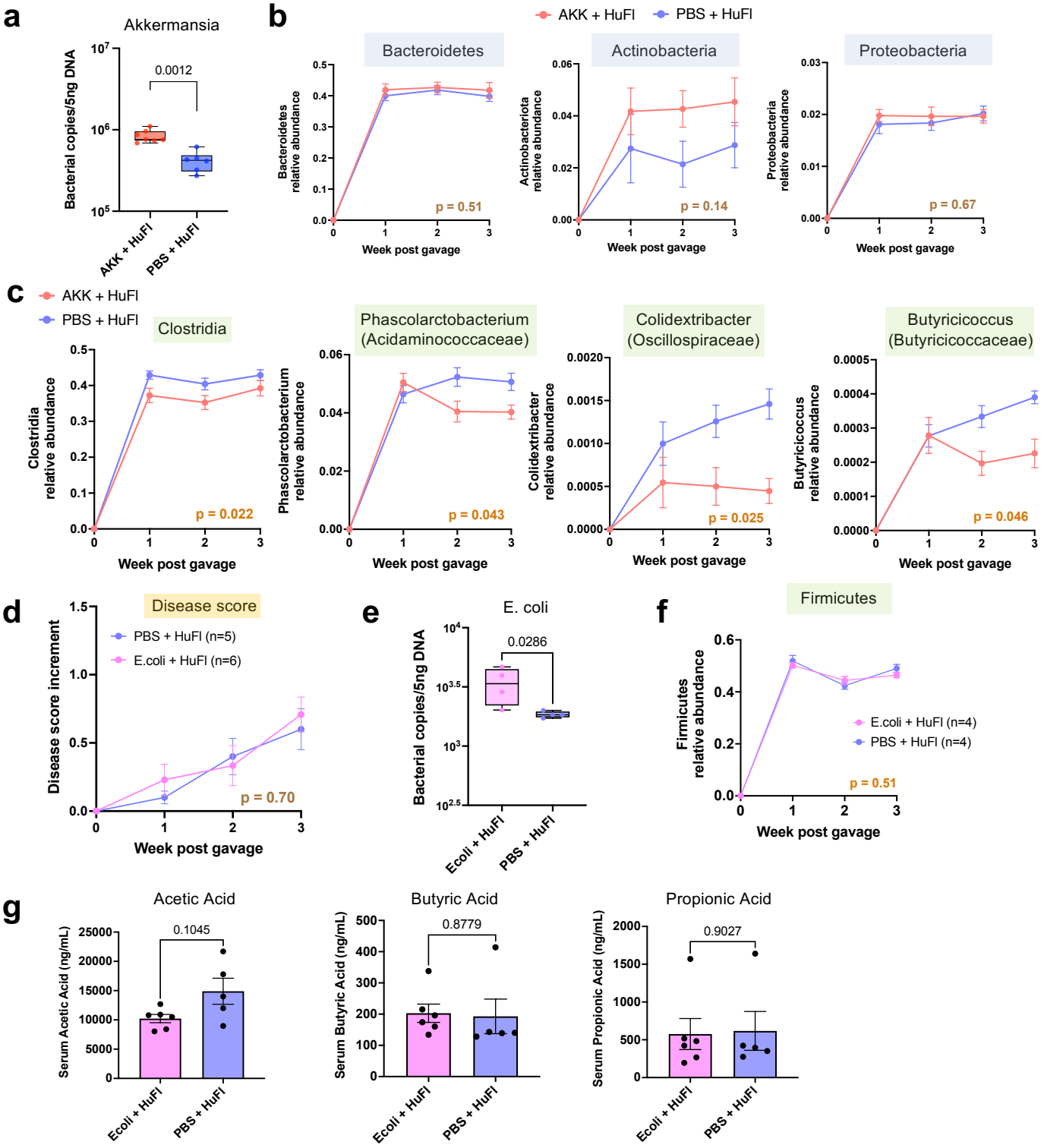
Extended Data Fig. 2 | Characterization of HuFl R161H gut microbiota and its disease association. a, Alpha diversity (Shannon Index) of gut content samples from mouse recipients, juxtaposed with stool samples from human donors. P < 0.0001 from Kruskal–Wallis test between mouse recipient groups, with p-values from Dunn's multiple comparisons shown in the plot. *n* = 77, 79, 78 for U, V, W mice, respectively. **b**–**c**, Venn Diagrams showing numbers of shared and unique bacterial taxa in fecal microbiome between each human and the recipient mouse cohort (**b**), and among three mouse cohorts (**c**). **d**, Average bacterial relative abundance in three mouse cohorts. Top 10 most abundant genera are shown. **e,** Alpha diversity (Shannon Index) of adult microbiome between female and male HuFl R161H (Wilcoxon rank sum test, p = 0.249). **f**, Beta diversity of adult HuFl R161H microbiome based on Bray–Curtis dissimilarity shows clustering by donor cohort rather than by sex. **g**, Multivariate taxonomic association with general linear models visualized as a dendrogram, showing bacterial taxa enriched in high (*n* = 16) or low (*n* = 24) histology categories in adult V-cohort R161H. Differentially abundant phyla and classes are labeled, FDR < 0.05. For **a**–**b**, each human donor sample has two technical replicates, and for **b**–**d**, *n* = 50, 59, 64 for mouse cohort U, V, W, respectively. For **e**–**f**, *n* = 44 and 61 for female and male, respectively (UVW combined).



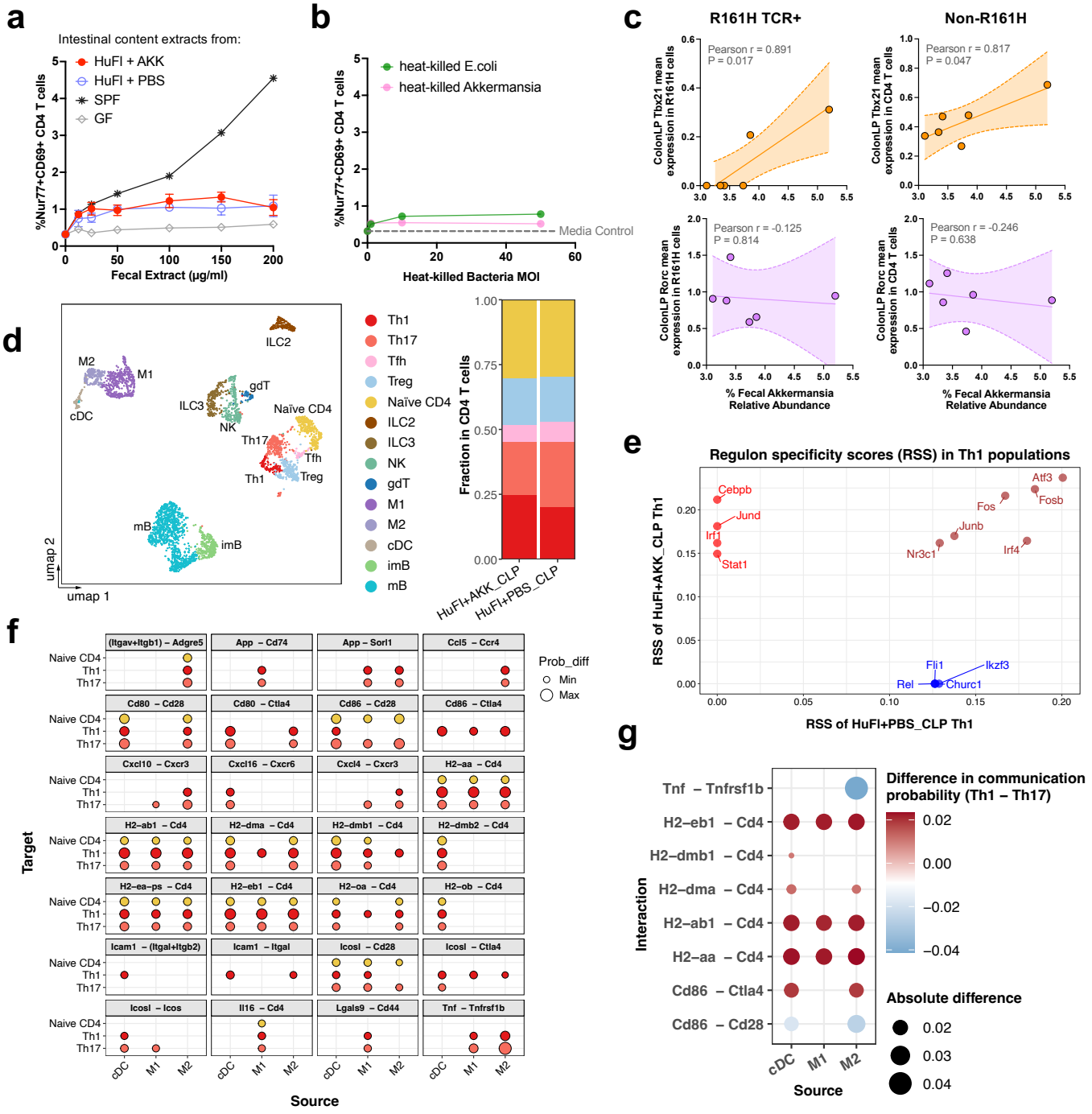
Extended Data Fig. 3 | Akkermansia – Firmicutes axis in HuFl R161H mice. a, Correlational heatmap showing associations of most abundant bacterial families (Firmicutes in green shade) with relative frequencies of colon LP CD4 T cells expressing each intracellular marker in adult HuFl R161H (n = 99, UVW combined). *P < 0.05, **P < 0.01, modeled by Spearman's rank correlation with Spearman's ρ defining the color gradient and circle size. **b**, Representative trend lines with 95% confidence interval (shaded area) show that relative Akkermansia abundance was positively associated with IFN-γ-producing, but not with IL-17A-producing, CD4 T cells in colon LP. **c**, Bacterial (family level) association networks in HuFl R161H mice (n = 234, UVW combined). Correlations with a threshold of Pearson r > 0.35 are shown. Node and edge color schemes same as in **Fig. 4**.



Extended Data Fig. 4 | Akkermansia promotes uveitis in the context of a minimal gut flora.
a, Experimental design of the "minimal flora model". **b**, Mean relative abundance of the two dominant fecal bacterial phyla, Firmicutes and Verrucomicrobiota, in AKK (n = 8) and PBS (n = 9) groups. **c**, Relative abundance of the top five fecal bacterial families in individual mice (represented by each column), two weeks after reconstitution. **d**, Fecal bacterial richness, a measure of alpha diversity, compared between AKK and PBS groups. **e**–**f**, Fundoscopy score increments from starting disease scores (**e**) and histology scores (**f**) of AKK and PBS mice. **g**, Relative abundance of Akkermansia and Firmicutes in feces, compared between AKK and PBS groups. **h**, A negative correlation of relative abundance between Akkermansia and Firmicutes by simple linear regression (n = 70, AKK and PBS groups combined, multiple time points included). **i**, Relative abundance of Actinobacteria and Proteobacteria in reconstituted mice. Bacteroidetes, another bacterial phylum that is normally abundant in the mouse gut, was nearly undetectable in these mice. Data are presented as mean values ± SEMs. P-value determined by Mann-Whitney U test in (**f**) and two-way ANOVA in (**d**, **e**, **g**, **i**). Results combined from two experiments. In plots with time series, microbial abundance at the time point "0" (GF status) represents a theoretical zero.



Extended Data Fig. 5 | Akkermansia promotes uveitis, while *E. coli* does not, in concert with base human flora. **a**, Absolute abundance of Akkermansia compared between Akk-rich and control mice two weeks after reconstitution. **b**, Relative abundance of major phyla Bacteroidetes, Actinobacteria and Proteobacteria **c**, Relative abundance of representative SCFA-producing Firmicutes (class to genus levels) in reconstituted mice (one representative experiment, n = 7 and 6 for Akk-rich and control, respectively). Data are presented as mean values ± SEMs. Statistical comparison between experimental groups was conducted using two-way ANOVA and p-values are shown in each graph. **d**–**g**, HuFl + E.coli (10^8 CFU) reconstitution experiments, as controls to Akkermansia. **d**, E.coli group did not develop more severe uveitis than PBS controls. **e**, Absolute abundance of E.coli one week after reconstitution. **f**, Relative abundance of Firmicutes. **g**, Serum concentrations of main SCFAs in E.coli-rich and control mice. Serum harvested four weeks post gavage. Data are presented as mean values ± SEM. Statistical comparison between experimental groups was performed using two-way ANOVA or Welch's t test.



Extended Data Fig. 6 | Akkermansia does not directly stimulate IRBP-specific T cells but can upregulate Th1 responses in the Akk-rich gut. **a**–**b**, Induction of Nur77 and CD69 expression in naïve IRBP-specific CD4 T cells from *Tcra*$^{-/-}$R161H-*Nr4a1*^{GFP} mice after 22 hours of stimulation with splenic dendritic cells (DC) from WT mice. Intestinal content extracts from R161H mice of indicated microbiome groups (**a**), and heat-killed Akkermansia or *E.coli* (**b**) were used as stimulants. GF (grey line in **a**) and media only (dotted line in **b**) represent baseline levels of activation. Multiplicity of Infection (MOI) is relative to DC. n = 4, 3 for HuFl+AKK and HuFl+PBS groups, respectively. **c**, Correlation of Akkermansia relative abundance at week 3 post-gavage with the normalized transcript abundance (*Tbx21* or *Rorc*) in R161H TCR-expressing and non-R161H CD4 T cells in the colon LP (CLP). Data from 5' single cell RNAseq from the Akkermansia reconstitution experiment, combined from HuFl+AKK (n = 3) and HuFl+PBS (n = 3) groups. **d,** UMAP of CD45^{+} cells from CLP of a representative mouse from each group, and proportions of CD4^{+} T cell subpopulations. Tfh, T follicular helper cells; ILC2/3, innate lymphoid cells; NK, natural killer cells; gdT, gamma delta T cells; M1/M2, macrophages; cDC, conventional dendritic cells; imB/mB, immature/mature B cells. **e,** Top 10 regulons enriched in Th1 cells in the CLP from representative HuFl+PBS (blue and brown) *vs.* HuFl+Akk (red and brown). Brown indicates regulons shared between groups. **f,** CellChat-inferred cell-cell communication in the CLP showing increased signaling from cDC and macrophages to naïve CD4 T and effector Th1 and Th17 cells in HuFl+Akk compared to HuFl+PBS. **g**, Differential signaling increases in Th1 cells compared to Th17 cells in HuFl+Akk gut.

Supplementary Files

This is a list of supplementary files associated with this preprint. Click to download.

- nrreportingsummary20251234696A.pdf